https://doi.org/10.15407/ujpe67.6.393

H. YASSIN,[1] A.N. TAWFIK,[2] E.R. ABO ELYAZEED [1]

[1] Physics Department, Faculty of Women for Arts, Science and Education, Ain Shams University
(Asma Fahmy St., Misr El Gedida, 11577 Cairo, Egypt)

[2] Future University in Egypt (FUE)
(End of Street 90, Fifth Settlement, 11835 New Cairo, Egypt; e-mail: a.tawfik@fue.edu.eg)

EXTENSIVE/NONEXTENSIVE STATISTICS FOR p_{T} DISTRIBUTIONS OF VARIOUS CHARGED PARTICLES PRODUCED IN $\mathrm{p}+\mathrm{p}$ AND $\mathrm{A}+\mathrm{A}$ COLLISIONS IN A WIDE RANGE OF ENERGIES

A comprehensive review on various experimental parametrizations proposed to fit the transverse momentum distributions of charged pions, kaons, and protons produced at energies ranging between 7.7 GeV and 2.76 TeV is introduced. We present a systematic study for their statistical fits to the extensive Maxwell–Boltzmann (MB) and nonextensive statistics (generic axiomatic statistics and the Tsallis one as a special case). The inconsistency that the MB approach is to be utilized in characterizing the chemical freezeout, while the Tsallis approach determining the kinetic freezeout is discussed. The resulting energy dependence of the different fit parameters largely varies with the particle species and the degree of (non)extensivity. This manifests itself in that the Tsallis nonextensive approach seems to work well for $p+p$, rather than for $A+A$ collisions. Nevertheless, discussing the deeper physical insights of nonextensive statistical approaches is not targeted, drawing a complete picture of the utilization of the Tsallis statistics in modeling the transverse momentum distributions of several charged particles produced at a wide range of energies and, accordingly, presenting a criticism or a support of the relevant works. This may be considered as the main advantage of this review.

K e y w o r d s: nonextensive thermodynamical consistency, genereic (non)extensive statistics, Boltzmann and Fermi–Dirac statistics.

1. Introduction

In high-energy collisions, large transverse momenta and particle yields are likely generated [1]. The statistical nature of such a particle production process was first proposed by Koppe [2]. In 1950, Fermi introduced first the solid statistical theory assuming the energy concentration in a small spatial volume which – through multiple successive processes – decomposes into many *smaller* final-state ones [3, 4]. Assuming a varying number of ideal particles including an aggregation of oppositely charged particles and satisfying the conservation laws, a generalization to quantum statistics was introduced by Magalinski and Terletskii in 1957 [5]. Based on a statistical bootstrap approach, Fast and Hagedorn introduced, in 1963, the mass spectrum function characterizing the abundances of the *so-far-detected* hadron resonances and introducing the concept of limiting temperature [6,7]. This very short overview highlights the key milestones of the use of the *extensive* Maxwell–Boltzmann statistics in high-energy collisions. Over the last five decades, enormous numbers of papers reporting on various statistical characteristics of the particle production have been published. Interested readers are kindly advised to consult recent review articles, such as Ref. [1]. There is a common consensus among particle physicists that the Maxwell–Boltzmann statistics describes well the particle multiplicities and their fluctuations and correlations within the so-far explored range of beam energies.

With the introduction of the Tsallis nonextensive statistics [8], different implications even in high-energy physics were proposed [9, 10]. This nonextensive approach assumes the same phase-space as in the *extensive* statistics, but it replaces the Boltzmann factors by the so-called q-exponential functions, with $q > 1$. A large number of research papers has been published so far dealing with this type of nonexten-

sivity, for instance, [9–24]. Recently, AT explained [25] that if one limits the Tsallis statistics nonextensivity to the related algebraic operations, one is apparently not assuring a proper implementation on the high-energy particle production. The possible interactions besides the fluctuations, the correlations, and the likely modifications in the phase space due to a symmetry change, for instance, seem not being incorporated through the q-statistics. In other words, a kind the global equilibrium seems being assumed no matter whether the energy varies, and/or the interacting system rapidly spatio-temporarily evolutes. To remain within the scope of the present research paper, we intentionally disregard the recent proposal that the degree of nonextensivity can be best considered. Instead of these types of nonextensivity, a wider class of superstatistics should be implemented, e.g., the generic nonextensive approach [25–27], where both Maxwell–Boltzmann and Tsallis approaches represent very special cases in it.

Nuclear physics, for instance, has a long history with the nonextensive statistics. Here, the nonextensive approaches are rightfully based on clear physical arguments. Weisskopf accounted for the fact that a high-energy emission reduces the temperature of the remaining nucleus [28]. This idea was extended to the canonical suppression of heavy ions [29,30]. The Tsallis-statistics-based arguments differ in that they are mainly useful to parametrize the nonextensivity, on one hand. On the other hand, they offer little physical insights. This research article reviews and discusses the Tsallis approach and focuses on its utilization in modeling the transverse momentum distributions of various charged particles produced in a wide range of energies. Not only the absence of deeper physical insights, but also the utilization itself seems not privileged a common agreement among the particle physicists.

Although the frequently reported surprising success of the Tsallis statistics in reproducing transverse momentum ($p_{\rm T}$) distributions of some charged particles in p + p collisions at high energies, various pieces of the puzzle are still missing [31–40]. For instance, the reproduction of $p_{\rm T}$ of the charged particles produced in A + A is mysteriously still overseen. Many colleagues believe that this is not as successful as in p + p collisions. In this regard, different questions should be answered, for example,

- a) whether the system size affects the possibility of the nonextensivity of such produced particles; mainly well-identified bosons and baryons representing low-lying Goldstone mesons and the most-stable fermions?
- b) whether the fits of the transverse momentum spectra of the various particles characterize the chemical or kinetic freezeout?
- c) whether the possible flow diminishes the proposed nonextensivity of these particles, when moving from p + p to A + A collisions?
- d) whether this *very special* type of nonextensivity is indeed able to describe the statistical nature of the particle production?

For example, if the answer to the last question, for instance, is "yes", one would expect that other aspects of the particle production, such as the particle multiplicity (particle yields and their ratios) could (should) be reproduced by the Tsallis statistics, as well. Apparently, this is not the case [25, 27, 41]!

The transverse momentum ($p_{\rm T}$) quantifies the projection of the four-momentum onto the plane with a transverse (perpendicular) orientation to the collision axis (z-axis). Accordingly, $p_{\rm T} = p\sin(\theta)$, where p is the four-momentum, and θ is the initial polar angle of the particle of interest with respect to the vertex position along the collision axis z. If the longitudinal momentum or rapidity (y) is integrated in the thermal distribution with no flow, the same $p_{\rm T}$-distribution can be obtained [42]. Studying the $p_{\rm T}$-distributions within thermal approaches gives – among others – an estimation for the temperature of the fireball (emission source) [43]. The transverse mass and energy can also be determined. The Tsallis distribution was utilized, for instant, to fit different particle spectra at the midrapidity from central d + Au, Cu + Cu, and Au + Au collisions at RHIC and p + Pb and Pb + Pb collisions at LHC energies [34]. Although the strong medium effects in nucleus-nucleus collisions (for example, Cu + Cu and Au + Au), it was concluded that the Tsallis approach can be used to fit most of the particle spectra in d + Au and p + Pb collisions, where the medium effects are assumed being very weak. In A + A collisions, the Tsallis approach is found capable to fit very well all the particle spectra at the RHIC energies except a little deviation observed for a proton and Λ at low $p_{\rm T}$ [34]. At LHC energies, the Tsallis distribution can only fit a part of the particle spectra either in a low or high $p_{\rm T}$ region. In order to reproduce

the entire $p_{\rm T}$ region, a new formula with an additional degree of freedom should be proposed, for instance,

$$\left(E\frac{d^3N}{dp^3}\right)_{|\eta|<a} = A\frac{\exp\left[-\frac{b}{T}\arctan\left(\frac{E_T}{b}\right)\right]}{\left[1+\left(\frac{E_T}{b}\right)^4\right]^c}, \tag{1}$$

where A, b, T, and c are free parameters. Expression (1) is inspired by the Fokker–Planck equation [44], where the exponent 2 is replaced by 4 [34]. The main idea proposed in Ref. [34] is that the transition from the exponential distribution to the Tsallis one should be conjectured to take place at intermediate $p_{\rm T}$. This proposed transition was done *ad hoc* in order to get a new expression to be used in fitting the intermediate $p_{\rm T}$ spectra from A + A collisions by accounting for the degrees of freedom greater than the ones available to the MB statistics.

Furthermore, a well-thorough study of the transverse momentum spectra of well-identified particles produced in p + p collisions at RHIC and LHC energies with the Tsallis distribution was conducted in Refs. [45, 46]. It was found that the rapidity and energy dependence of the $p_{\rm T}$ spectra in p + p collisions describes well the experimental results from STAR, PHENIX, ALICE, and CMS programs [35]. This becomes possible, when the cascade particle production mechanism was included. The energy dependence of the temperature (T) and q (where q is thought similar as the parameter n) of the Tsallis distribution has been discussed in detail [35].

It should be noted that almost all relevant experimental results are detectable differential quantities, such as $dN/d^3p = \int d^3p(p^\mu/p^0)f_0(x,p)$, satisfying normalization conditions, so that the total number, for instance, reads

$$N = \int\limits_S \frac{dN}{d^3p}d^3p = \int\limits_S n(x)u^\mu d\sigma_\mu, \tag{2}$$

where $f_0(x,p)$ is the phase-space distribution function, S is the surface, $d\sigma_\mu$ is a time-like normal vector, and u^μ is the four velocity. Similarly, the transverse momentum and the transverse momentum distribution, respectively, can be expressed as

$$p_{\rm T} = \int_S \frac{dN}{d^3p}p^x d^3p = \int_S T^{\mu x}d\sigma_\mu, \tag{3}$$

$$\frac{dN}{p_{\rm T}dp_{\rm T}} = \gamma V\int\frac{d^3p}{p^0}\frac{d[p^\mu u_\mu f(x,p)]}{p_{\rm T}dp_{\rm T}}, \tag{4}$$

where $T^{\mu x}$ is the energy-momentum tensor.

The present paper focuses on a comprehensive characterization of the transverse momentum distributions of various charged particles produced in p + p and A + A collisions at beam energies ranging between 7.7 GeV and 2.76 TeV. We also present a short review on the various experimental parametrizations, where measured $p_{\rm T}$ are well fitted, but not necessarily within q-statistics of the Tsallis type, for instance. We shall discuss the possible reasons for that this type of nonextensivity seems to be successful for p + p but not for A + A collisions! In addition, we will highlight that the resulting fit parameters are not only depending on the energy, but – among others – on the particle species, themselves!

2. Approaches

2.1. Statistical-thermal approaches

2.1.1. Transverse momentum distributions

a. Extensive statistics. As proposed in the literature [10, 39], the four-momentum in the nonrelativistic limit, i.e., $m \gg p$, could be replaced by the transverse momentum ($p_{\rm T}$), the transverse mass [$m_{\rm T} = (p_{\rm T}^2 + m^2)^{1/2}$], and the rapidity ($y$), with the dispersion relation $E = m_{\rm T}\cosh(y)$, so that $d^3p = p_{\rm T}\,m_{\rm T}\,\cosh(y)\,dp_{\rm T}\,dy\,d\phi$, where ϕ is the azimuthal angle. At a finite temperature (T), the chemical potential (μ), and volume (V) and assuming a full detector acceptance, i.e., $\int d\phi = 2\pi$, the extensive Maxwell–Boltzmann (MB) and Fermi–Dirac and Bose–Einstein (F|B) statistical approaches, respectively, give

$$\frac{1}{2\pi p_{\rm T}}\left.\frac{d^2N}{dp_{\rm T}\,dy}\right|_{\rm MB-extensive} = \frac{gV}{(2\pi)^3}\,m_{\rm T}\,\cosh(y)\times$$
$$\times\,\exp\left(\frac{\mu - m_{\rm T}\,\cosh(y)}{T}\right), \tag{5}$$

$$\frac{1}{2\pi p_{\rm T}}\left.\frac{d^2N}{dp_{\rm T}\,dy}\right|_{\rm F|B-extensive} = \pm\frac{gV}{(2\pi)^3}\,m_{\rm T}\,\cosh(y)\times$$
$$\times\left[\exp\left(\frac{m_{\rm T}\,\cosh(y)}{T} - \mu\right)\pm 1\right]^{-1}, \tag{6}$$

which can be derived straightforwardly from the distribution function in the corresponding four-space,

$$N|_{\rm MB-extensive} = gV\int\limits_0^\infty \frac{d^3p}{(2\pi)^3}e^{\frac{\mu-\varepsilon}{T}}, \tag{7}$$

$$N|_{\mathrm{F|B-extensive}} = \pm gV \int_0^\infty \frac{d^3p}{(2\pi)^3} \frac{e^{\frac{\mu-\varepsilon}{T}}}{1 \pm e^{\frac{\mu-\varepsilon}{T}}}, \tag{8}$$

where $\varepsilon = (p^2 + m^2)^{1/2}$ is the extensive dispersion relation in natural units, g is the degeneracy factor and μ combine all types of chemical potentials.

b. Tsallis and Tsallis factorized nonextensive statistics. For the sake of simplicity, the Tsallis statistics is applied to the Maxwell–Boltzmann distributions, Eq. (7). Accordingly, the total number of particles can be estimated within the Tsallis nonextensive statistics as follows:

$$N = gV \int_0^\infty \frac{d^3p}{(2\pi)^3} \left[1 + (q-1)\frac{E-\mu}{T}\right]^{\frac{-q}{q-1}}, \tag{9}$$

where $q > 1$ is the key parameter defining the degree of Tsallis nonextensivity. The dependence of q on T, μ, and $\sqrt{s_{\mathrm{NN}}}$ shall be reviewed later on. The four-momentum distribution can be expressed as

$$E\frac{d^3N}{d^3p} = E\frac{gV}{(2\pi)^3} \left[1 + (q-1)\frac{E-\mu}{T}\right]^{\frac{-q}{q-1}}. \tag{10}$$

At a finite chemical potential and a non-vanishing rapidity, the transverse-momentum distribution reads

$$\frac{1}{2\pi p_{\mathrm{T}}} \left.\frac{d^2N}{dp_{\mathrm{T}}dy}\right|_{\mathrm{Tsallis-nonexten.}} = V\frac{g}{(2\pi)^3} m_{\mathrm{T}} \cosh(y) \times \times \left[1 + (q-1)\frac{m_{\mathrm{T}}\,\cosh(y) - \mu}{T}\right]^{-q/(q-1)}. \tag{11}$$

When $q \to 1$, Maxwell–Boltzmann statistics can be resembled, straightforwardly [8, 10], Eq. (5). The upper bound on q is naturally set by the given derivatives [10]. Per definition, both expressions describe an ideal nonextensive gas, i.e., one can sum over the constituents of such an additive gas. On the other hand, the given single-particle multiplicity distribution is conjectured to be used in a powerful modeling of the transverse momentum distribution of the individual produced particle [10]. It was argued that many-particle multiplicity distributions using the Tsallis statistics does not factorize into a product of single-particle ones [47]. It was pointed out that only a factorization approximation allows the use of an explicit single-particle distribution function in the Tsallis statistics [48]

$$\frac{1}{2\pi p_{\mathrm{T}}} \left.\frac{d^2\,N}{dp_{\mathrm{T}}\,dy}\right|_{\mathrm{factorized}} = V\frac{g}{(2\pi)^3}\, m_{\mathrm{T}}\, \cosh(y) \times \times \sum_{N=0}^{N_0} \frac{\tilde{\omega}^N}{N!}\, h_0(N) \times \times \left[1 + \frac{q-1}{q}\frac{\Lambda - m_{\mathrm{T}}\,\cosh(y) - \mu(N+1)}{T}\right]^{-\frac{q}{q-1}+3N}, \tag{12}$$

where $\tilde{\omega} = gVT^3/\pi^2$,

$$h_0(N) = \begin{cases} \dfrac{[q/(1-q)]^{3N}\Gamma[1/(1-q) - 3N]}{\Gamma[1/(1-q)]}, & q < 1, \\ \dfrac{[q/(q-1)]^{3N}\Gamma[q/(1-q)]}{\Gamma[q/(q-1) + 3N]}, & q > 1. \end{cases} \tag{13}$$

and the norm function Λ is to be determined from a norm equation [47]. It was concluded that, at SPS energies, where the entropic parameter gets a value very close to unity, the Tsallis factorized statistics, Eq. (12), seems to deviate from the Tsallis non-factorized statistics, Eq. (11). At higher energies, both types of the Tsallis statistics become indistinguishable [47]. This result strengthens the argumentation that the implementation of Tsallis approach on particle production at top RHIC and LHC energies should be carefully conducted [25, 27].

At $y = 0$ (mid-rapidity), Eqs. (11)–(12) can be reformulated [10, 47]. Also, for a given rapidity range $y_0 < y < y_1$, the transverse momentum distribution can be extended to include an integration over dy [10, 47]. For a systematic fit of p_{T} distributions, we highlight that some experimental measurements are normalized to the geometrical factor $2\pi p_{\mathrm{T}}$, while others are not. This might affect the given experimental uncertainties. We disregard this slight difference while comparing to our calculations.

c. Generic and generic-factorized nonextensive statistics. To introduce a generalized statistical approach to a large statistical system having various types of nonextensivity, such as the particle production at high energies, two asymptotic properties, each is associated with a scaling function, have been proposed [26]. Each scaling function is characterized by one critical exponent. These are c for the first property and d for the second one, by which an equivalence class of entropies can be defined uniquely:

$$S_{c,d}[p] = \sum_i^\Omega \mathcal{A}\Gamma(d+1, 1 - c\ln p_i) + \mathcal{B}p_i, \tag{14}$$

where Ω is the number of states, $\Gamma(a,b) = \int_b^\infty dt\, t^{a-1} \exp(-t)$ being incomplete Γ-function, and $\mathcal{A}$ and $\mathcal{B}$ are arbitrary parameters. In the limit $\Omega \to \infty$, each admissible system approaches one of these equivalence classes. It was concluded [26] that the universality classes (c,d) not only introduce the generic entropy and characterize it entirely, Eq. (14), but also specify the particle distribution functions,

$$f_{c,d,r}(x) = \exp\left[-\frac{d}{1-c}\mathtt{W}_k\left(B\,(1-x/r)^{1/d}\right)\right] \times \\ \times \exp\left[\frac{d}{1-c}\mathtt{W}_k(B)\right], \tag{15}$$

where $\mathtt{W}_k$ is k-th branch of the Lambert-W function, which has real solutions at $k=0$ for all classes with $d \geq 0$ and at $k=-1$ for $d<0$, as well. $B \equiv \equiv (1-c)r/[1-(1-c)r]\, \exp\{(1-c)r/[1-(1-c)r]\}$ with $r = (1-c+cd)^{-1}$. At $k=0$, the asymptotic expansion of the Lambert-W function reads

$$\mathtt{W}_{k=0}(x) = \sum_{n=1}^{\infty} \frac{(-1)^{n-1}\, n^{n-2}}{(n-1)!}\, x^n. \tag{16}$$

The properties of this new (non)extensivity entropy, Eq. (14), lead to

$$\frac{1}{1-c} = \lim_{N\to\infty} N\, \frac{\Omega'}{\Omega}, \tag{17}$$

$$d = \lim_{N\to\infty} \log\Omega\, \left(\frac{1}{N}\frac{\Omega}{\Omega'} + c - 1\right), \tag{18}$$

while the number of microstates (Ω) is related to the distribution function

$$\Omega(N) = \frac{1}{f_{c,d}(-\varphi\, c\, N)} \times \\ \times \exp\left\{\frac{d}{1-c}\mathtt{W}_k\left(\frac{(1-c)\exp\left[\frac{1-c}{c}\, d\right]}{c\, d}\, \left[\frac{\varphi\, c\, N}{r}\right]^{\frac{1}{d}}\right)\right\}, \tag{19}$$

where φ is given by

$$\varphi = \frac{d}{dN}\, S_g = \Omega'\, \left(g(1/\Omega) - \frac{1}{\Omega}\, g'(1/\Omega)\right). \tag{20}$$

For the Maxwell–Boltzmann distribution, the probability can be expressed as

$$p_i = \frac{1}{z}\, f_{c,d,r}(x_i), \tag{21}$$

where $f_{c,d,r}(x_i)$ was given in Eq. (15) and the partition function can be constructed as follows:

$$z = \sum_i f_{c,d,r}(x_i). \tag{22}$$

At a finite temperature (T) and a finite chemical potential (μ), the single-particle distribution function reads

$$\langle n_{p\sigma}\rangle = \frac{1}{z} \sum_{\{n_{p\sigma}\}} \frac{n_{p\sigma}}{\prod_{p\sigma} n_{p\sigma}!} f_{c,d,r}\left(\sum_{p\sigma} n_{p\sigma} X\right) = \\ = f_{c,d,r}(x_p), \tag{23}$$

where $x_p = (\epsilon_p - \mu)/T$, $\sum_{n_{p\sigma}} n_{p\sigma}\, f = f_p$, if $x \to x_p$ and

$$f_{c,d,r}\left(\sum_{\{n_{p\sigma}\}} x\right) = \exp\left\{\frac{-d}{1-c}\left[W_k\left(B\left(1 + \frac{\Lambda}{rT} - \right.\right.\right. \\ \left.\left.\left. - \sum_{n_{p\sigma}} \left(\frac{E_p - \mu}{T}\right)\right)^{1/d}\right) - W_k(B)\right]\right\}. \tag{24}$$

Then, the partition function can be given as

$$z = \sum_{\{n_{p\sigma}\}} \frac{1}{\prod_{p\sigma} n_{p\sigma}!}\, f_{c,d,r}\left(\sum_{p\sigma} n_{p\sigma} X\right) = \\ = \exp\left(\sum_{p\sigma} \langle n_{p\sigma}\rangle\right). \tag{25}$$

The conversion from classical to quantum statistics is straightforward:

$$z = \pm \sum_{\{n_{p\sigma}\}} \frac{1}{\prod_{p\sigma} n_{p\sigma}!} \times \\ \times \left[f_{c,d,r}\left(1 \pm \sum_{p\sigma} n_{p\sigma} X\right)^{-1}\right], \tag{26}$$

where $\pm$ represent fermions and bosons, respectively.

The averaged number reads

$$\langle N\rangle = \sum_{n_{p\sigma}} \langle n_{p\sigma}\rangle. \tag{27}$$

To estimate the norm function for the proposed generic nonextensive statistics,

$$\sum_{\{n_{p\sigma}\}} \frac{1}{\prod_{p\sigma} n_{p\sigma}!}\, f_{c,d,r}\,(x_i) = 1, \tag{28}$$

we start with

$$\sum_{N=0}^{\infty}\int_{0}^{\infty} dE\, f_{c,d,r}\,(x)\; W_{N,E} = 1, \tag{29}$$

where

$$W_{N,E} = \sum_{\{n_{p\sigma}\}} \frac{1}{\prod_{p\sigma} n_{p\sigma}!}\delta\left(\sum_{p\sigma} n_{p\sigma} - N\right) \times$$

$$\times\delta\left(\sum_{p\sigma} n_{p\sigma}\epsilon_p - E\right), \tag{30}$$

$$E = \sum_{n_{p\sigma}} \langle n_{p\sigma}\rangle\, \epsilon_p. \tag{31}$$

In a grand canonical ensemble of a Maxwell–Boltzmann ideal gas, this might be reexpressed as

$$W_{N,E} = \frac{1}{N!}\left(\frac{gV}{\pi^2}T^3\right)^N \frac{E^{3N-1}}{\Gamma(3N)}. \tag{32}$$

Then, the transverse momentum distribution can be expressed as

$$\frac{1}{2\pi p_{\rm T}}\frac{d^2N}{dydp_{\rm T}} = \frac{gVT}{8\pi^3} m_{\rm T}\cosh y \sum_{N=0}^{N_0}\frac{\tilde{\omega}^N}{N!}\frac{h_0(0)}{r(1-c)} \times$$

$$\times W_0\left[B\left(1+\frac{\Lambda}{rT} - \frac{m_{\rm T}\cosh y - \mu(N+1)}{rT}\right)^{1/d}\right] \times$$

$$\times\left[T + \Lambda - m_{\rm T}\cosh y + \mu(N+1)\right] \times$$

$$\times\left\{1+W_0\left[B\left(1+\frac{\Lambda}{rT} - \frac{m_{\rm T}\cosh y - \mu(N+1)}{rT}\right)\right]^{\frac{1}{d}}\right\}, \tag{33}$$

where

$$\tilde{\omega} = \frac{gVT^3}{\pi^2}, \tag{34}$$

$$h_0(0) = \begin{cases} \dfrac{\left(\frac{c}{1-d}\right)^{3N}\Gamma\left(\frac{1}{1-d}-3N\right)}{\Gamma\left(\frac{d}{1-d}\right)} & \text{at } d<1, \\ \dfrac{\left(\frac{c}{d-1}\right)^{3N}\Gamma\left(\frac{c}{d-1}\right)}{\Gamma\left(\frac{c}{d-1}+3N\right)} & \text{at } d>1. \end{cases} \tag{35}$$

2.1.2. $p_{\rm T}$ spectra and kinetic freezeouts

In this section, we discuss whether the $p_{\rm T}$ spectrum distributions are to be related to the chemical freezeout or to the kinetic one. The former is a late stage of the temporal evolution of high-energy collisions at which the particle abundances can be described by the equilibrium distribution functions determined by – at least – a set of three types of parameters, namely, the temperatures (T), the baryon chemical potentials (μ), and the fireball volumes (V). The number of produced particles is likely fixed, i.e., no further *chemical* processes take place or no longer change in the produced particles. At this stage, the produced particles would exist in their ground states, as well as in various excited states. The kinetic freezeout is conjectured to take place at lower temperatures, e.g., the system cools down during a very late stage of the colliding system. The corresponding *effective* temperature describes the degree of excitation of the *elastically* interacting system. It is conjectured that, during this stage, the thermal equilibrium in which the $p_{\rm T}$ spectrum distributions of the produced particles are no longer changed, is apparently reached. As mentioned, distinguishing between these two phases is a great objective to be achieved. We review recent studies aiming at proposing answers to the question which quantitatively characterizes which stage?

From the statistical fits of the $p_{\rm T}$ spectrum distributions, various thermal parameters including the fireball geometry and the expansion velocity could be extracted. As elaborated in the previous section, extensive and nonextensive approaches were frequently utilized to characterize the particle production and, though indirectly, to model the final state of the interacting system [1]. Alternatively, this can also be achieved through the *direct* comparison with calculations based on the multisource thermal model, single freezeout scheme [49], and the incoherent-multiple-collision model [50], for instance. It was pointed out [51] that both Blast-wave [52] and thermal fireball models [53] seem not capable to model the $p_{\rm T}$ momentum spectra. Models inspired by hydrodynamics [54] are assumed to propose a good estimation for the kinetic freezeout parameters; kinetic temperature ($T_{\rm kin}$), and the average transverse radial flow velocity [$\langle\beta\rangle = 2\beta_S/(2+n)$], where β_S is the surface velocity, and n is the exponent of the flow profile and thus offer the fruitful information about the collision dynamics. Such models propose that the produced par-

ticles are locally thermalized at $T_{\rm kin}$ and flow with a common $\langle\beta\rangle$,

$$\frac{dN}{p_{\rm T}dp_{\rm T}} \propto \int\limits_0^R r\,dr\,m_{\rm T}\,I_0\left(\frac{p_{\rm T}}{T_{\rm kin}}\sinh\rho(r)\right)\times$$
$$\times\,K_1\left(\frac{m_{\rm T}}{T_{\rm kin}}\cosh\rho(r)\right), \qquad (36)$$

where $m_{\rm T}=(p_{\rm T}^2+m^2)^{1/2}$ is the transverse mass with m being the mass of the particle of interest. I_0 and K_1 are the modified Bessel functions. $\rho(r)=\tanh^{-1}\beta$, where $\beta=\beta_S(r/R)^n$, and r/R is the relative radial position in the thermal source. It should be noted that some of these approaches assume an extensive statistics.

It is apparent that the produced particles are considerably affected by the dynamics of the interacting system. Various observations support unambiguously this conclusion. With these regards, it was noticed that the shape of the momentum distributions depend on the freezeout hypersurface [55]. From a hydrodynamic description, i.e., modeling the system as an expanding hadron fluid, both strength and duration of the expansion can be characterized, and an effective equation of state could be determined [56].

Another finding connected with the statistical fits of the $p_{\rm T}$ momentum spectra is the so-called nonextensive effective temperature [25, 57]. Following the proposal that the effective temperature differs from the real temperature, both effective and real temperatures were extracted from the mean transverse flow velocity and the mean flow velocity of produced particles [58]. Their dependence on rest and moving masses, centralities, and center-of-mass energies could be extracted, as well [58–60]. It was argued that both types of temperatures can be related to each other [25]. Such an extrapolation shall be elaborated in Section 2.4.

2.2. Empirical parametrizations

This section reviews another alternative that the transverse momentum $p_{\rm T}$ distributions of different charged particles produced at various energies can be fitted statistically without conciliating to a sprcific statistical approach. On one hand, experiments mostly aim at a best description of their results apart from the possible complications and the constraints of some theoretical approaches. On the other hand, the resulting parametrizations for different $p_{\rm T}$ distributions become precise, so that they turn to offer excellent descriptions for the characterization of the $p_{\rm T}$ distributions. For a better comparison, we divide the various experimental parametrizations according to the system sizes.

2.2.1. AA collisions

It is well known that the STAR experiment – among others – runs a successful program for the $p_{\rm T}$ distributions of the well-defined charged particles ($\pi^{\pm}$, $K^{\pm}$, p, and $\bar{p}$) produced in Au + Au collisions [61, 62]. Recently, a systematic beam energy scan at 7.7, 11.5, 19.6, 27, and 39 GeV was reported [61] for $0.2 < p_{\rm T} < < 2$ GeV. These results are depicted in Figs. 12–16. The results at higher energies shall be discussed as well. First, we introduce three examples on parametrizations proposed by the STAR collaboration [61]. At mid-rapidity $y < 0.1$ and in $({\rm GeV/c})^2$ units, the $p_{\rm T}$ distributions have been fitted to Bose–Einstein, $m_{\rm T}$-exponential, and double-exponential, respectively,

$$\frac{1}{2\pi p_{\rm T}}\frac{d^2N}{dp_{\rm T}\,dy}=c_{\rm BE}\left[\exp\left(\frac{m_{\rm T}}{T_{\rm BE}}\right)-1\right]^{-1}, \qquad (37)$$

$$\frac{1}{2\pi p_{\rm T}}\frac{d^2N}{dp_{\rm T}\,dy}=c_{m_{\rm T}}\exp\left[\frac{-(m_{\rm T}-m)}{T_{m_{\rm T}}}\right], \qquad (38)$$

$$\frac{1}{2\pi p_{\rm T}}\frac{d^2N}{dp_{\rm T}\,dy}=c_1\exp\left(\frac{-p_{\rm T}^2}{T_1^2}\right)+c_2\exp\left(\frac{-p_{\rm T}^2}{T_2^2}\right). \qquad (39)$$

Other parametrizations such as Boltzmann $\propto m_{\rm T}\exp(-m_{\rm T}/T)$ and $p_{\rm T}$-exponential $\propto\exp(-p_{\rm T}/T)$ have been proposed as well [61]. It is obvious that these expressions suggest various power-scales. Depending on the resulting parameters, which are summarized in Tables 1, 2, one would be able to favor one or another power-scale. It would be of great interest to compare between them and the ones proposed by the Tsallis statistics. The latter is blindly applicable in low, as well as in high p_T regions and, therefore, was categorically criticized, for instance, in ref. [63]. We also compare these fits with the ones using the same parametrizations but at the energies 62.4, 130, and 200 [62]. The results are added to Tables 1, 2 as well.

Tables 1, 2 summarize the results on the proportionality constants (c) and the inverse slopes (T) deduced from statistical fits of Bose–Einstein, Eq. (37), $m_{\rm T}$-exponential, Eq. (38), and double-exponential

functions, Eq. (39) to the p_{T} spectra measured in the STAR experiment in 0–5% collisions for pions, Kaons, and protons and their antiparticles, respectively. It is obvious that the inverse slopes, T, of the p_T spectra of pions are smaller than that of the kaons, which in turn are smaller than that of the protons. It is obvious that

• there is a general pattern observed that T increases with the center-of-mass energies,

• the resulting T of pions, kaons, and protons (particles) p_{T} spectra are slightly greater than that of their counterparts (antiparticles), respectively, and

• especially for protons and antiprotons, the increase of T with the center-of-mass energies might be monotonic except at 19.6 GeV or at 27 GeV, where a rapid increase or decrease is registered. This region of the center-of-mass energies shall be precisely scanned in the forthcoming energy scan program of the STAR experiment. It might reveal interesting new physics!

Table 1. **Proportionality constants (c) and inverse slopes (T) obtained from the statistical fits of p_{T} spectral distributions for the well-identified pions, kaons, protons, and their antiparticles measured in Au + Au central collisions (0–5%) at the mid-rapidity ($y < 0.1$) and energies of 7.7, 11.5, 19.6, 27, and 39 [61] to Bose–Einstein [Eq. (37)], m_{T}-exponential, Eq. (38), and double-exponential functions, Eq. (39), respectively**

Particle	Parameter	7.7 GeV	11.5 GeV	19.6 GeV	27 GeV	39 GeV
π^+	c_{BE} GeV^{-2}	331.804	398.084	479.707	493.251	474.231
	T_{BE} GeV	0.204	0.211	0.217	0.222	0.230
π^-	c_{BE} GeV^{-2}	370.501	433.36	498.458	521.712	497.888
	T_{BE} GeV	0.200	0.207	0.216	0.220	0.227
K^+	$c_{m_{\mathrm{T}}}$ GeV^{-2}	20.981	24.475	27.561	28.117	28.159
	$T_{m_{\mathrm{T}}}$ GeV	0.221	0.227	0.234	0.240	0.245
K^-	$c_{m_{\mathrm{T}}}$ GeV^{-2}	8.662	13.099	18.165	21.645	22.070
	$T_{m_{\mathrm{T}}}$ GeV	0.203	0.212	0.228	0.230	0.244
p	c_1 GeV^{-2}	20.923	17.462	7.949	10.947	1.533
	$T1$ GeV	0.905	0.899	0.999	0.947	1.218
	c_2 GeV^{-2}	19.429	49.943	6.136	0.009	7.641
	$T2$ GeV	0.00062	0.00500	0.72454	0.02321	0.89727
$\bar{p}$	c_1 GeV^{-2}	0.154	0.579	1.490	0.0026	2.819
	T_1 GeV	0.907	0.894	0.945	0.0024	0.981
	c_2 GeV^{-2}	0	0	0.000095	2.070	0.00011
	T_2 GeV	0.40511	0.51028	0.08611	0.96683	0.09363

Table 2. **The same as in Table 1, but at 62.4, 130, and 200 [62]**

Particle	Parameter	62.4 GeV	130 GeV	200 GeV
π^+	c_{BE} GeV^{-2}	575.202	167.267	422.939
	T_{BE} GeV	0.250	0.236	0.259
π^-	c_{BE} GeV^{-2}	741.325	159.963	560.647
	T_{BE} GeV	0.228	0.230	0.243
K^+	$c_{m_{\mathrm{T}}}$ GeV^{-2}	155.855	80.419	192.892
	$T_{m_{\mathrm{T}}}$ GeV	0.269	0.250	0.275
K^-	$c_{m_{\mathrm{T}}}$ GeV^{-2}	137.548	63.217	178.744
	$T_{m_{\mathrm{T}}}$ GeV	0.270	0.250	0.275
p	c_1 GeV^{-2}	5.205	2.870	2.957
	$T1$ GeV	0.822	0.827	0.980
	c_2 GeV^{-2}	2.202	0.336	0.046
	$T2$ GeV	1.193	1.249	1.095
$\bar{p}$	c_1 GeV^{-2}	2.323	1.463	1.523
	T_1 GeV	0.851	0.880	0.928
	c_2 GeV^{-2}	1.208	0.370	1.074
	T_2 GeV	1.179	1.224	1.084

For the nonextensive Tsallis and generic axiomatic statistics, we note that

• the temperature T increases with the center-of-mass energies except (with an exception at 200 GeV) for all particles except for pions,

• for pions, there is the inverse proportionality between T and $\sqrt{s_{\mathrm{NN}}}$, and

• the resulting T from p_{T} spectra of the antiparticles are slightly greater than that from p_{T} spectra of their particles.

It is obvious that the resulting temperatures range between 0.204 and 0.245 GeV for pions and kaons. But for protons, there are two sets of resulting temperatures, the first term of Eq. (39) results in $0.894 < T < 1.218$ GeV, while the second term gives $0.00062 < T < 0.96683$ GeV.

For pions and kaons, the temperatures determined are found greater than the freezeout temperatures which means that both transverse momentum spectra are nearly stemming from the hadronization phase. But in the case of protons, the temperatures are very large. There is a huge difference between these and the freezeout temperatures. Accordingly, we conclude that the transverse momentum distributions for protons are likely to be stemming from the quark hadron transition phase, i.e., earlier than the hadronization phase.

On the other hand, we note that the proportionality constants seem to have a monotonic increase with the center-of-mass energy, especially for pions and kaons, but not for protons, especially at 19.6 GeV or at 27 GeV. This would be interpreted as that, at these two energies, both thermal and chemical freeze-out temperatures likely exceed the one deduced from the Blast-wave and thermal models, respectively. In other words, the overestimation becomes greater at 19.6 GeV or at 27 GeV pointing to the new physics that both sets of statistical approaches become distinguishable. This is another phenomenological observation supporting the idea that this energy range deserves a finer analysis. Future facilities such as the Facility for Antiproton and Ion Research (FAIR) at GSI, Darmstadt, Germany and the Nuclotron-based Ion Collider fAcility (NICA) at JINR, Dubna, Russia are designed – among others – to cover such an energy range. The RHIC Beam Energy Scan program in the STAR experiment targets this energy region as well.

Prior to the results reported in Ref. [61], STAR collaboration published the detailed p_{T} spectrum distributions of $\pi^{\pm}$, $K^{\pm}$, p and $\bar{p}$, at 62.4, 130, and 200 GeV in Au–Au collisions at the mid-rapidity [62]. Besides the parametrizations based on p_{T}-exponential, m_{T}-exponential, and Boltzmann expressions, other expressions have been proposed, as well such as p_{T}-Gaussian and p_{T}^3-exponential,

$$\frac{dN}{p_{\mathrm{T}}\,dp_{\mathrm{T}}} = c_{p_{\mathrm{T}}^2} \exp\left(-\frac{p_{\mathrm{T}}^2}{T_{p_{\mathrm{T}}^2}^2}\right), \tag{40}$$

$$\frac{dN}{p_{\mathrm{T}}\,dp_{\mathrm{T}}} = c_{p_{\mathrm{T}}^3} \exp\left(-\frac{p_{\mathrm{T}}^3}{T_{p_{\mathrm{T}}^3}^3}\right). \tag{41}$$

We would like to emphasize that the parameters in Eqs. (37)–(39) are determined and listed out in Tables 1, 2.

Table 3 shows the results on the effective temperatures as determined from the charged particles and their antiparticles in central Au + Au collisions at 62.4, 130, and 200 GeV [62] by using the parametrizations given in Eqs. (37), (38), (39), (40), (41). We note that, for all such particles and antiparticles, there is an increase of the effective temperatures with the energies. On the other hand, the results for pions are lower than the ones for Kaons, which in turn are lower than the ones for protons and antiprotons.

2.2.2. $p + p$ collisions

Due to the non-Abelian energy loss of parent parton penetrating through a dense medium (jet quenching), which is likely available in A + A collisions, the possible suppression in the high p_{T} spectra of leading hadrons, such as pions, kaons, and protons in A + A compared to p + p collisions was proposed as canonical signatures for the QGP formation [64]. While it was concluded [65] that the high p_{T} spectra of hadrons produced in central Au + Au collisions at 3 tops of RHIC energies, $\sqrt{s_{NN}} = 130$, and 200 GeV,

Table 3. **The proportionality constants (c) and the inverse slopes (T) obtained from the statistical fits of p_{T} spectral distributions for the well-identified pions, kaons, protons, and their antiparticles measured in Au + Au central collisions (0–5%) at the mid-rapidity ($y < 0.1$) and energies 62.4, 130, and 200 GeV [62] by using different parametrizations given in Eqs. (37), (38), (39), (40), (41)**

Particle	Parameter	62.4 GeV	130 GeV	200 GeV
π^+	$c_{p_{\mathrm{T}}}$-exponential GeV^{-2}	897.773	1071.82	1128.81
	$T_{p_{\mathrm{T}}}$-exponential GeV	0.1996	0.201	0.209
π^-	$c_{p_{\mathrm{T}}}$-exponential GeV^{-2}	916.824	1086.12	1175.46
	$T_{p_{\mathrm{T}}}$-exponential GeV	0.1996	0.201	0.206
π^+	c_{BE} GeV^{-2}	759.95	938.961	937.542
	T_{BE} GeV	0.21	0.208	0.22
π^-	c_{BE} GeV^{-2}	702.611	840.006	856.455
	T_{BE} GeV	0.221	0.2213	0.233
K^+	$c_{m_{\mathrm{T}}}$ GeV^{-2}	184.534	201.305	149.856
	$T_{m_{\mathrm{T}}}$ GeV	0.27	0.284	0.322
K^-	$c_{m_{\mathrm{T}}}$ GeV^{-2}	159.003	178.227	124.089
	$T_{m_{\mathrm{T}}}$ GeV	0.27	0.284	0.35
p	c_1 GeV^{-2}	3.119	2.738	3.055
	T_1 GeV	0.982	0.991	1.107
	c_2 GeV^{-2}	4.98	4.233	4.125
	T_2 GeV	1.19	1.324	1.438
$\bar{p}$	c_1 GeV^{-2}	2.32	1.462	1.523
	T_1 GeV	1.122	1.182	1.2
	c_2 GeV^{-2}	1.33	3.44	4.102
	T_2 GeV	1.2	1.224	1.25
p	$c_{p_{\mathrm{T}}}$-Gaussian GeV^{-2}	8.103	6.879	7.079
	$T_{p_{\mathrm{T}}}$-Gaussian GeV	1.101	1.225	1.278
$\bar{p}$	$c_{p_{\mathrm{T}}}$-Gaussian GeV^{-2}	3.535	4.798	5.503
	$T_{p_{\mathrm{T}}}$-Gaussian GeV	1.188	1.248	1.266

are found strongly suppressed by a factor of 4–5 [66–71] comparing to the results from p + p-collisions at the same energies [69, 72], it was reported that the high $p_{\rm T}$ spectra of pions produced in central A + A-collisions at CERN-SPS energies are enhanced relative to their p + p counterparts [73–78].

The latter would manifest the *"Cronin effect"* in the hadron production, which was first observed in 1975 [79] and effectively refers to an enhancement in the high $p_{\rm T}$ spectra due to multiple interactions of (anti)particles produced in pA and A + A collisions, e.g., bound nucleons seem to accumulate leading to the high $p_{\rm T}$ spectra of the leading hadrons. On the other hand, the suppression observed at the top of RHIC energies can be understood due to two phenomena [80]. The first one is the multiple interactions within the colliding heavy-ions, *"Cronin effect"*. The second one describes the final-state interactions with the dense medium. Accordingly, the dense medium properties could be characterized, when the Cronin effect for such nuclear collisions can be determined, precisely.

From this short review on the results of the high $p_{\rm T}$ from p + p and A + A collisions, we are now able to summarize that the suppression and the enhancement of $p_{\rm T}$ spectra of the leading hadrons measured in A + A-collisions relative to the ones in p + p collisions sheds light on the Cronin effect, the medium modification and signatures for the QGP formation, in the nuclear matter. Let us firstly recall some proposals for the dynamics behind the Cronin effect. A parameter-free approach which describes well the available experimental data was suggested in Ref. [80]. It is based on the assumption that the mechanism of the multiple interactions should be affected by the collision energy, on the one hand. At low collision energies, high $p_{\rm T}$ of partons are incoherently produced off different nucleons, while, at high collision energies, their production becomes coherent, i.e., the coherence length, the distances along a projectile momentum direction, linearly increases with the energy [81]

$$l_c = \frac{\sqrt{s_{\rm NN}}}{m_{\rm N}\, k_{\rm T}}, \tag{42}$$

where $k_{\rm T}$ is the transverse momentum of the parton which is produced at mid-rapidity. Later on, such partons likely undergo the confinement phase transition forming hadrons that shall be detected and their $p_{\rm T}$ measured. This expression could be interpreted by means of the Heisenberg uncertainty principle and the QCD renormalizability as follows [82]. If l_c becomes shorter than the averaged internucleon separation, then the projectile interacts incoherently with individual nucleons similar to the p + p scattering; otherwise, the interaction is coherent [82, 83]. On the other hand, if the coherence length becomes short, then the possible broadening in the $p_{\rm T}$ spectrum distribution [84], which might be produced due to initial and/or final interactions, should not be interpreted as a medium effect on the parton distribution of the nucleus [80]. The possible broadening in momentum spectra was proposed as a signature for the QGP formation [84]. If l_c becomes longer than the nuclear radius, it is conjectured that all amplitudes, for instance, of λ's of x's, interfere, coherently [82,83]. This leads to a collective parton distribution for the nucleus. The amplitudes with large parton momentum related to large $l_c \sim (m_{\rm N} x)^{-1}$ likely overlap and, thus, have no correlations with individual nucleons. This means that the factorization can be applied, while the parton distribution becomes modified [85, 86].

We have briefly reviewed the reproduction of the $p_{\rm T}$ spectra measured in A + A and p + p collisions at the top of RHIC energies and at SPS ones. A strong suppression is found in the former, while an enhancement is to be concluded in the latter [65]. For the sake of completeness, we recall that the Cronin effect could be well confirmed in fixed target pA-collisions at Fermilab energies of 20–40 GeV [87, 88] and in $\alpha\alpha$-collisions at ISR energies of about 31 GeV [89].

Now, we can review the various parametrizations for $p_{\rm T}$ distributions:

• First, we recall the five-parameter functional form for the inclusive cross-section distribution at ISR energies [65]

$$E\frac{d^3\,\sigma_{\rm pp\to\pi X}}{dp^3} = A\left[\exp\left(ap_{\rm T}^2 + bp_{\rm T}\right) + \frac{p_{\rm T}}{p_0}\right]^{-n}, \tag{43}$$

where $A = 265.1$ mb GeV^{-2}, $a = -0.0129$ GeV^{-1}, $b = 0.049$ GeV, $p_0 = 2.639$ GeV, and $n = 17.95$.

• Second, from the different parametrizations utilized at 0.9, 2.76 and 7 TeV, we start with the modified Hagedorn function. This was utilized by the ALICE collaboration for a better parametrization for low $p_{\rm T}$ differential cross-sections [90],

$$\frac{1}{2\pi p_{\rm T}}\,\frac{d^2\sigma^2_{\rm ch}}{dp_{\rm T}\,d\eta} = A\frac{p_{\rm T}}{m_{\rm T}}\left(1 + \frac{p_{\rm T}}{p_{\rm T,0}}\right)^{-n}, \tag{44}$$

where n is a q-like exponent. It was concluded that this expression behaves itself, at high $p_{\rm T}$, as a power law (asymptotic), while, at low $p_{\rm T}$, the quantities within the brackets, $(1 + p_{\rm T}/p_{\rm T,0})^{-n}$, represent the exponential function with an inverse slope parameter $p_{\rm T,0}/n$. The differential cross section, in left-hand side, $d^2\sigma^2_{\rm ch}/dp_{\rm T}\,d\eta$, was measured as $\sigma^{\rm NN}_{\rm MB_{OR}}$ multiplied by the number of charged particles per event differential yield of charged particles in minimum bias collisions, $d^2N^{\rm MB_{OR}}_{\rm ch}/dp_{\rm T}\,d\eta$.

• Third, the ALICE results on differential cross-sections have been confronted to NLO-pQCD calculations [91]. The scaling exponent n was estimated by comparing the spectra $x_{\rm T} = 2p_{\rm T}/\sqrt{s_{\rm NN}}$ at different center-of-mass energies $\sqrt{s_{\rm NN}}$ and $\sqrt{s'_{\rm NN}}$ for fixed $p_{\rm T}$,

$$n(x_T) = -\frac{\ln\left[\sigma_{\rm inv}(s_{\rm NN}, x_{\rm T})/\sigma_{\rm inv}(s'_{\rm NN}, x_{\rm T})\right]}{\ln(\sqrt{s_{\rm NN}}/\sqrt{s'_{\rm NN}})}, \qquad (45)$$

where the quantities with prime are the ones compared to the quantities without prime.

• Fourth, the LHC results on $p_{\rm T}$ spectra of well-identified and unidentified particles have been parametrized as well [92–96]. The generic parametrization reads

$$\frac{d^2N}{dy\,dp_{\rm T}} = p_{\rm T}\,\frac{dN}{dy}\,\frac{(n-1)(n-2)}{nT[nT+(n-2)m]}\times$$
$$\times\left[1+\frac{m_{\rm T}-m}{nT}\right]^{-n}, \qquad (46)$$

where n is an exponent (though being equivalent to the Tsallis q parameter), and T gives the inverse slope parameter (equivalent to the temperature). dN/dy is the yield distribution. From experimental point-of-view, the systematic errors count possible contributions from all individual detectors, overall normalization errors, and the uncertainties in the extrapolation to large $p_{\rm T}$. For pions, which are the lowest Goldstone bosons and, accordingly, more abundant than other particles, at the midrapidity, $p/E \equiv p_{\rm T}/m_{\rm T}$. Accordingly, the rhs of the previous expression should be multiplied by $p_{\rm T}/m_{\rm T}$ for pions, especially. This type of parametrization is known as Tsallis–Pareto or Tsallis–Levy [97]. Through a private communication, Tsalli rejected that this has any thing to do with the Tsallis statistics. The various fit parameters are detailed in the Tables 4 and 5 of Ref. [93]. For the sake of comparison, we give, in Table 4, the results of Ref. [93].

2.3. Other models for $p_{\rm T}$ spectral distributions

Assuming that many emission sources are formed in the high-energy collisions, a multisource thermal model with different interacting mechanisms and different detection samplings has been proposed [98–100]. It was conjectured that the sources of one group are in a local equilibrium. This allows one to apply singular distributions and to assign, to the multisources, one common temperature and the same degrees of freedom as well. It is apparent that the emission of the produced particles off the multisources constructs the final-state spectrum, which can be characterized statistically by a multicomponent distribution law [101]. In light of this, the authors of Ref. [102] proposed that a multicomponent Erlang $p_{\rm T}$ spectral distribution estimates the mean $p_{\rm T}$ of each group, and the Tsallis statistics determines the effective temperature of the whole interacting system, which may have group-by-group fluctuations in different local thermal equilibria. To this end, we recall firstly the assumption that the particles generated off one emission source obey the exponential function of $p_{\rm T}$ spectral distribution [58, 100]

$$f_{ij}(p_{{\rm T}_{ij}}) = \frac{1}{\langle p_{{\rm T}_{ij}}\rangle}\,\exp\left[\frac{p_{{\rm T}_{ij}}}{\langle p_{{\rm T}_{ij}}\rangle}\right], \qquad (47)$$

where $p_{{\rm T}_{ij}}$ is $p_{\rm T}$ spectra stemming from the i-th source in the j-th group and $\langle ...\rangle$ gives the mean value. When summing up over N_j sources in the j-th group, the single-component Erlang distribution could be constructed as

$$f_j(p_{\rm T}) = \frac{p_{\rm T}^{N_j-1}}{(N_j-1)!\,\langle p_{{\rm T}_{ij}}\rangle^{N_j-1}}\,\exp\left[\frac{p_{{\rm T}_{ij}}}{\langle p_{{\rm T}_{ij}}\rangle}\right], \qquad (48)$$

where $p_{\rm T}$ stands for the transverse momentum contributed by N_j sources. When summing up over all groups, the multicomponent Erlang distribution is obtained:

$$f_E(p_{\rm T}) = \sum_{j=1} w_j\, f_j(p_{\rm T}), \qquad (49)$$

where w_j is the relative weight of the j-th group. The mean transverse momentum reads

$$\langle p_{\rm T}\rangle = \sum_{j=1} w_j\, N_j \langle p_{{\rm T}_{ij}}\rangle. \qquad (50)$$

It was assumed that the temperature deduced from the multicomponent Erlang and Tsallis fits to the

mean and transverse spectra of various produced particles at RHIC and LHC energies is identical to the kinetic one characterizing the thermal freezeout [58]. The flow velocity could also be extracted. Various colliding systems including p + p, Cu + Cu, Au + Au, Pb + Pb, and p + Pb at different centralities have been analyzed [58]. To all these systems, the multisource thermal model was also utilized. The effective temperature and the real (physical) temperature could be determined. The latter is likely identical to the thermal freezeout temperature of the interacting system. The mean transverse flow velocity and the mean flow velocity of produced particles, as well as relationships among these quantities, were extracted as well. Furthermore, this extensive study determined the dependence of the effective temperature and the mean and transverse momentum distributions on the rest mass, the moving mass, the centrality, and the center-of-mass energy. In addition, the dependence of the thermal freezeout temperature and the mean and the transverse flow velocity on the centrality, center-of-mass energy, and system size was analyzed [58].

The rapidity and the energy dependence of the transverse momentum spectra for charged particles in $p - p$ collisions were analyzed using two types of Tsallis approaches, e.g., with and without thermodynamic description, where experimental results from the STAR, PHENIX, ALICE, and CMS experiments could be well reproduced [32]. It was found that the temperatures obtained with the thermodynamic description are smaller than the ones without such description [32]. In the Tsallis distribution with thermodynamical descriptions, there is an extra term m_T which is responsible for the discrepancies of the temperatures from the other type of Tsallis approaches.

The experimental results from light flavor particles; p, π, K, and their antiparticles measured in Au + Au at 200 GeV and from strange particles; K^0_S, Λ, Ξ, Ω measured in Cu + Cu at 200 GeV are confronted to the multisource thermal model. On the other hand, we find that the results of p, π^+, K^+, ϕ from Pb + Pb at 2.76 TeV, as well as $\pi^+ + \pi^-$, $K^+ + K^-$, $p + \bar{p}$, $\Lambda + \bar{\Lambda}$, K^0_S from p + Pb at 5.02 TeV, and p, π^+, K^+, Λ, ϕ, $\Sigma^- + \bar{\Sigma^+}$ at 0.9 and 7 TeV from p + p collisions, which apparently combine different colliding systems and different energies, are well described by means of the standard Tsallis approaches, e.g., the ones compelling with the Fermi–Dirac or Bose–Einstein statistics and with the two- and three-component standard distributions [103]. From this analysis, a dependence of the effective temperature on the rest mass of the particle m_0 was proposed [103]. The proposed relation between the effective temperature T also expressed as T_{T-S} or T_T, or T_S and the particle's rest mass m_0 is given as [104–108]

$$T = T_0 + a\, m_0, \tag{51}$$

where T_0 is intercept also given as T_{T-S_0}, or T_{T_0}, or T_{S_0} of the linear relation between T and m_0 at $m_0 = = 0$. In addition, T_0 is known as the kinetic freezeout temperature of interacting system.

The transverse momentum spectra of pions, kaons, and proton and their antiparticles at the midrapidity in p + p collisions at 7 TeV measured by the ALICE experiment have been analyzed by using different techniques [109, 110]. This allows the precise measurements within different p_{T}-ranges including low for pions and moderated range for both kaons and protons [109]. The dependence of the results from Pb + Pb collisions at 2.76 TeV on the particle mass was parametrized by using MB Blast-wave fits [110]. Various collective phenomena in small colliding systems such as central p + p and p + Pb and peripheral Pb + Pb have been investigated.

Furthermore, the relativistic stochastic model in the three-dimensional (non-Euclidean) rapidity space was used to describe the transverse momentum spectra for antiprotons from Au + Au collisions. The radial symmetric diffusion in the Euclidean space reads [111]

$$\frac{\partial f}{\partial t} = \frac{D}{\sinh^2 y} \frac{\partial}{\partial y} \left[\sinh^2 y \frac{\partial f}{\partial y} \right], \tag{52}$$

where D is the diffusion constant. Under initial conditions, we get

$$f(y, t = 0) = \frac{\delta(y - y_0)}{4\pi \sinh^2 y}. \tag{53}$$

The coincidence between the relativistic stochastic model and the Maxwell–Boltzmann one is found at $k_{\mathrm{B}} T = = m\sigma(t)^2$, where k_{B} is the Boltzmann constant, and $\sigma(t)^2 = 2DT$. So, the temperatures could be estimated from the Maxwell–Boltzmann distribution function at low and high p_{T}-ranges under the assumption that, in the lower momentum limit, the distribution function approaches the Maxwell–Boltzmann one, when the rapidity becomes smaller than unity ($y \ll 1$) or $p_T \ll m$ [111].

2.4. Extrapolation to the Boltzmann temperature

As discussed in Sec. 2.3, the effective temperature can be expressed in terms of the particle' rest mass, Eq. (51) [103]. Thus, the intercept T_0 (known as T_{T-S_0}, T_{T_0}, or T_{S_0}) gives the temperature at the kinetic freezeout of the interacting system or the real temperature (source) [104–108]. Alternatively, T_0 could be understood as the quantity related to a massless particle. Furthermore, the parameter a can be given as a function of the $v_0^2/2$, where v_0 is the transverse radial flow velocity [105, 106]. It was concluded that $a = v_0^2/2$ is only valid within the low $p_{\rm T}$-region [105, 106]. On the other hand, $a = v_0^2/2$ within $p_{\rm T} > 2$ GeV/c would be only valid, if the radial flow velocity becomes modified v_{T-S0}, or v_{T0}, or v_{S0} corresponding to the Tsallis-standard and Tsallis apprpaches or even to the standard distributions. The latter include the standard Boltzmann, Fermi–Dirac, and Bose–Einstein distributions, which can be summarized as

$$f_i(p_{\rm T}) = \frac{1}{N}\frac{dN}{dp_{\rm T}} = C_{i0} p_{\rm T} \sqrt{p_{\rm T}^2 + m_0^2} \int\limits_{y_{\rm min}}^{y_{\rm max}} \cosh y \times$$

$$\times \left[\exp\left(\frac{\sqrt{p_{\rm T}^2 + m_0^2}\cosh y}{T_i} \right) + S \right]^{-1} dy, \qquad (54)$$

where C_{i0} is the normalization constant [103], and T_i is the effective temperature for the i-th component. Furthermore, it was concluded that T_{T-S}, T_T, and T_S increase with the collision centrality, and $T_{T-S} \leq T_T < T_S$ for a given set of data [103].

The two-Boltzmann, where $i = 2$ in Eq. (54) and the Tsallis distributions have been utilized in studying the transverse momentum distributions of the final-state particles produced in high-energy collisions at LHC energies [112]. It was found that the resulting two temperatures refer to fluctuations taking place in the interacting system. The temperature fluctuations have been investigated under the consideration of an interacting system of groups with different sizes. Other observables such as the transverse energy and the multiplicity have been related to these fluctuations. The Tsallis statistics seem to describe well the temperature fluctuations and the degree of non-equilibrium. The latter is merely referring to a change in the nonextensivity parameter q. Thus, this study has showed that the Tsallis statistics describes well the fluctuations in both T and q. From two-Boltzmann distributions, the temperature of the interacting system T can be given as [33]

$$T = k_1 T_1 + k_2 T_2, \qquad (55)$$

where k_1 and k_2 are constants denoting the contributions from the first and second Boltzmann distributions, respectively. Alternatively, the temperature of the interacting system can be given as $T = k_1 T_1 + (1 - k_1) T_2$ [112].

The transverse momentum spectra of the charged particle produced in Au + Au collisions at RHIC energies and in Pb + Pb collisions at LHC ones with different centrality intervals were analyzed by the multisource thermal model in which the Tsallis distributions, the Boltzmann distributions (two-component), Tsallis distributions, and the (two-component) Boltzmann distributions are implemented [33]. It was concluded that there is a linear correlation between the effective temperatures obtained from both Tsallis and Boltzmann distributions,

$$T_{\rm T} = (0.956 \pm 0.009) T_{\rm B} + (-0.034 \pm 0.004). \qquad (56)$$

$T_{\rm T}$ refers to the Tsallis temperature, while $T_{\rm B}$ refers to the Boltzmann temperature.

In Au + Au collisions at RHIC energies, it was concluded that the effective temperatures $T_{\rm T}$ and $T_{\rm B}$ increase with the particle masses, but decrease with the increasing in the centrality. The comparison between the two types of temperatures results in $T_{\rm T} < T_{\rm B}$ and also helps in estimating the nonextensive parameter q. It was found that the latter is almost not changing in most cases [33].

From the values obtained for the effective temperatures for charged particles measured in Pb + Pb collisions at 2.76 TeV, it was noticed that both $T_{\rm T}$ and $T_{\rm B}$ increase with the particle masses, but they are not depending on the centrality of the collisions, especially, when moving from central to semicentral collisions. In addition, it was found that $T_{\rm T} < T_{\rm B}$, but q does not depend on the centrality of the collisions. On the other hand, q slightly increases from semicentral to peripheral collisions [33].

The transverse momentum spectra of strange particles produced in Pb + Pb, p + Pb, and $p - p$ collisions at different center-of-mass energies with different multiplicities which measured by the CMS experiment have been described by using both Tsallis

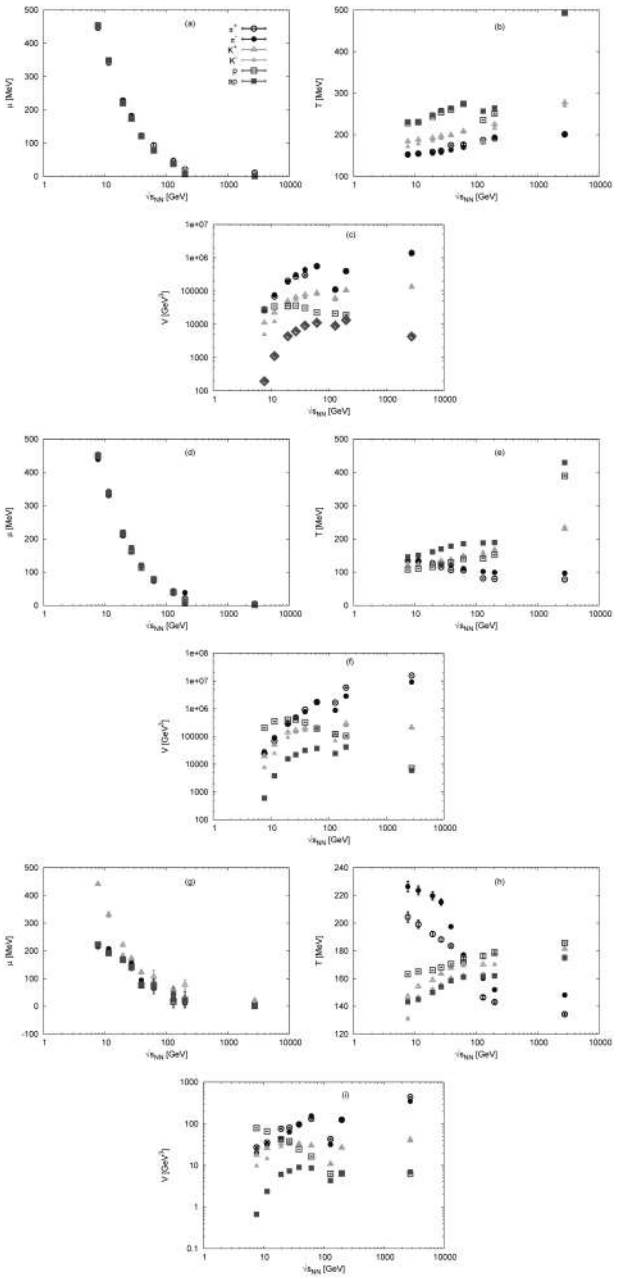

Fig. 1. The various parameters obtained from the statistical fits within the Boltzmann, Tsallis, and generic axiomatic statistics for p_{T} measured in A + A collisions for various charged particles in a wide range of energies, Appendices A.1.a, A.1.b, A.1.c

and Boltzmann statistics [113]. The effective temperatures, the Tsallis temperature (T_{Ts}), and the Boltzmann temperature (T_{Boltz}) are found increasing with both the mass and strangeness number of the particles and also increasing with the multiplicities, but q decreasing with the increase in the particle' mass and also decreasing with the increase in the multiplicities. There is a linear correlation between the extracted temperatures from the two types of statistics

$$T_{\mathrm{Ts}} = aT_{\mathrm{Boltz}} + b, \tag{57}$$

where $a = 1.2465 \pm 0.0138$ and $b = -160.499 \pm 5.386$. So, the two temperatures were found related to each other as $T_{\mathrm{Ts}} < T_{\mathrm{Boltz}}$. The values of the constants a and b change with a change in the particle mass as

$$\text{For } K_s^0 \quad T_{\mathrm{Ts}} = (1.3714 \pm 0.0092)\, T_{\mathrm{Boltz}} + \\ + (-177.514 \pm 2.503). \tag{58}$$

$$\text{For } \Lambda \quad T_{\mathrm{Ts}} = (1.3856 \pm 0.0255)\, T_{\mathrm{Boltz}} + \\ + (-209.84 \pm 10.2). \tag{59}$$

$$\text{For } \Xi^- \quad T_{\mathrm{Ts}} = (1.39513 \pm 0.0212)\, T_{\mathrm{Boltz}} + \\ + (-249.213 \pm 9.963). \tag{60}$$

3. Results

3.1. Statistical-thermal approaches

3.1.1. A + A Collisions

Figure 1 shows the fit parameters for the charged particles and antiparticles as functions of the center-of-mass energies in A + A collisions obtained from three types of statistics, namely, Boltzmann (top panels), Tsallis (medium panel), and generic statistics (bottom panel). These parameters are the chemical potential μ (left panel), the temperature T (medium panel), and the volume V (right panel). We note that the chemical potential is inversely proportional to the center-of-mass energies for all particles. This is valid for the different types of statistics. For the Boltzmann statistics, the temperature increases with the energies for all particles. For both Tsallis and generic statistics, the temperature increases, as well with the energies for kaons and protons and their antiparticles; but, for pions, it decreases. With respect to the volume. We note that the volume increases with the energies for all particles except for proton (here, the volume decreases with the energies).

Figure 2 presents the nonextensive parameters q and d for the Tsallis and generic statistics as functions of the center-of-mass energies for charged particles and antiparticles. We find in the left panel that q

decreases with the increase in energies for kaons and protons, but increases for pions. On the other hand, d decreases with the increase in the center-of-mass energies for all particles and antiparticles.

From the resulting (c, d) that $c = 0.999506$ and remains unchanged, while d is positive, but less than unity, let us review the right panel of Fig. 5, i.e., $(c, d) \equiv (1, d > 0)$. We conclude that this result is stretched exponentials and asymptotically stable classes of entropy. In this particular case, this means that

$$S_\eta(p) = \sum_i \Gamma\left(\frac{\eta+1}{\eta}, -\ln p_i\right) - p_i\Gamma\left(\frac{\eta+1}{\eta}\right), \qquad (61)$$

where $\eta = 1/d$ is characterized as a stretching exponent distribution, i.e., $\eta > 0$ [114]. At positive d, the branch of Lambert-W functions, which are the real solutions of $x = W_k(x)\exp(W_k(x))$, is the one at $k = 0$ defined by the solutions of $W_0(x) \sim x - x^2 + \ldots$. Within the given η-region, there are three cases:

- at $\eta < 1$, S_η, known as superadditive,
- at $\eta > 1$, S_η known as subadditive, and
- at $\eta = 1$, S_η is characterized by positivity, equiprobability, concavity, and irreversibility.

The third case means that the first three Shannon–Khinchin axioms, i.e., the continuity, the maximality, and the expandability, besides the extensivity are verified. This reproduces the *logarithmic* MB nonextensive entropy. As an example, let us assume that $(c, d) \equiv (1, 2)$, where $\eta = 1/2$. Then, we get that

$$S_{1,2}(p) = 2\left(1 - \sum_i p_i \ln p_i\right) + \frac{1}{2}\sum_i p_i \left(\ln p_i\right)^2. \qquad (62)$$

This is a superposition of two entropy terms. Furthermore, it is apparent that $S_{1,2}(p)$ is superadditive, and its asymptotic behavior is dominated by the second term.

Coming back to the stretched exponent distributions, which are characterized by $c \to 1$, we recall that the MB extensive entropy is to be recovered at $d = 1$. In addition, the Tsallis nonextensive entropy is to be restored, at $d = 0$. The Lambert exponential is given as

$$\lim_{c\to 1} \varepsilon_{c,d,r}(x) = \exp\left\{-dr\left[(1 - x/r)^{1/d} - 1\right]\right\}, \qquad (63)$$

where $r = (1 - c + cd)^{-1}$ determining the distribution function, especially at small probabilities of microstates (x); but not effecting the asymptotic properties. The values obtained for the two equivalent classes (c, d) make it suitable to recall their physical meaning and their relation to (non)equilibrium mechanism. Interested readers are advised to consult Ref. [115].

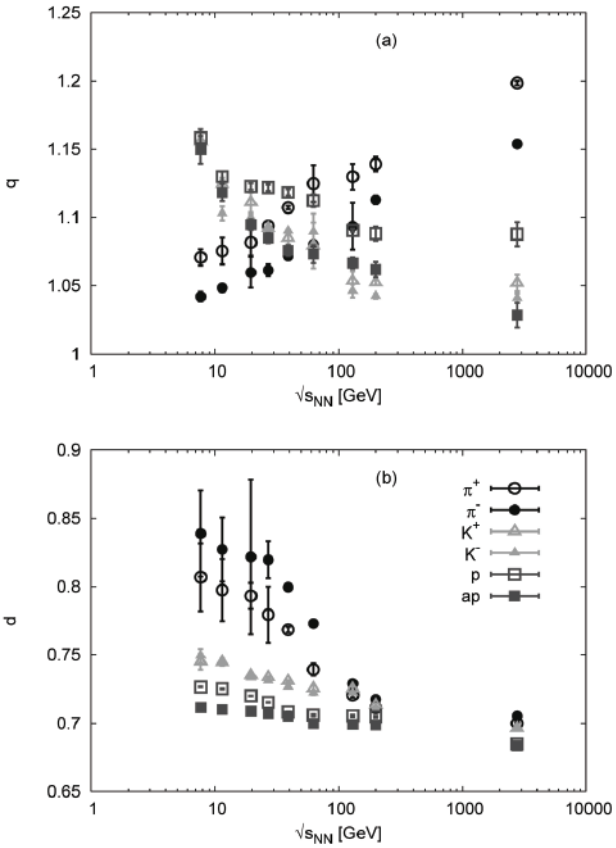

Fig. 2. The nonextensive parameters q and d obtained from statistical fits within the Tsallis and generic axiomatic statistics, respectively, for p_T measured in A + A collisions, Appendices A.1.b, A.1.c

Figure 3 depicts the fit parameters obtained from the three types of statistics as functions of the center-of-mass energies. Left panel shows a comparison for pions, middle panel illustrates kaons, while right panel presents protons and antiprotons. Top panel gives the dependence of μ on center-of-mass energies. An inverse proportionality between μ and the energies for all particles using all types of statistics is obtained. Middle panel shows the temperature as a function of the energies. It is to be noted that the temperature increases with the energies for kaons and

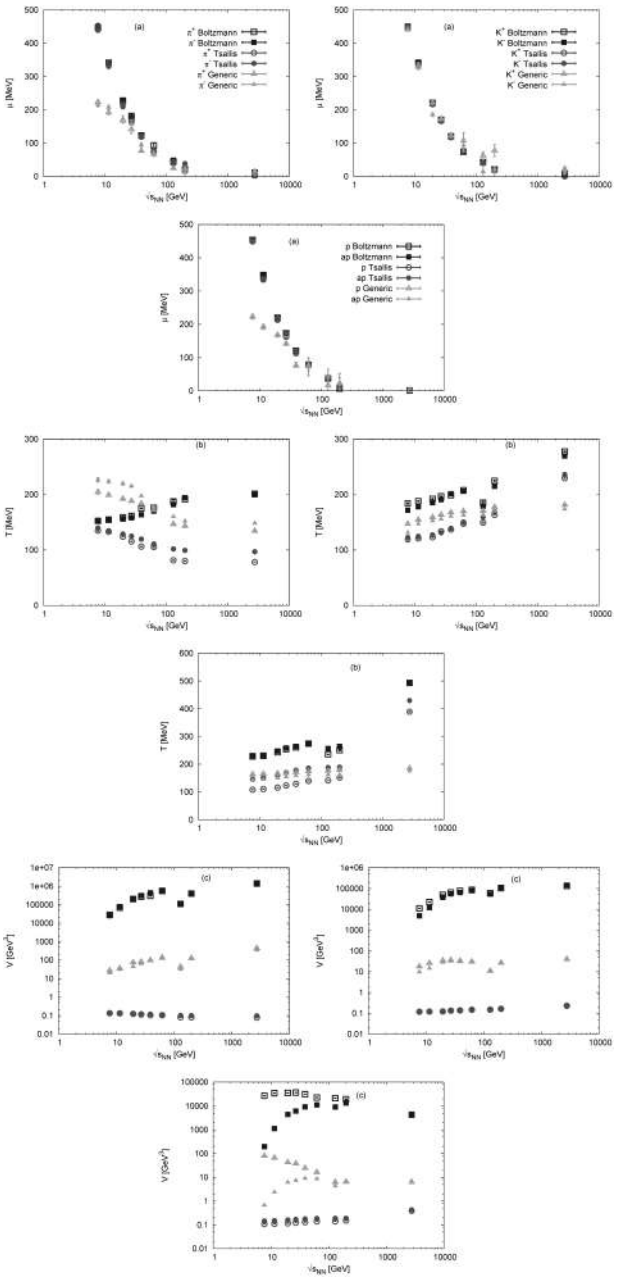

Fig. 3. A comparison between μ, T, and V obtained from the statistical fits within the Boltzmann, Tsallis, and generic axiomatic statistics for p_{T} measured in A + A collisions for various charged particles in a wide range of energies, compared with Fig. 1 and Appendices A.1.a, A.1.b, A.1.c

protons from the three types of statistics, while this dependence is only obtained using the Boltzmann statistics for pions. By using a nonextensive statistics, we find that the temperature of pions decreases with the increase in energies. Bottom panel presents the dependence of the volume on the center-of-mass energies. We find that the volume increases with the energies for pions and kaons using the three types of statistics. For protons (antiprotons), such a dependence is only obtained when using the Tsallis statistics. But, for protons with the use of the Boltzmann and for protons and their antiparticles by using the generic statistics, the volume is found decreasing with the increase in the energies.

We conclude that, by using the Boltzmann statistics, there is a general behavior that the temperature increases with the energies for all particles. At 200 GeV, the temperature has values smaller than the ones at lower energies. We conclude that the temperature obtained from antiparticles are slightly greater than the ones for the particles. But, for a nonextensive statistics, the temperature increases with the energies for all particles except for pions. Another exception for pions could be highlighted that there is a reverse proportionality between the temperature and the energies. The resulting temperature from p_{T} spectra of antipions, antikaons, and antiprotons are slightly greater than that from p_{T} spectra of their particles.

3.1.2. p + p Collisions

Figure 4 depicts the fit parameters for the charged particles and antiparticles as functions of the center-of-mass energies in p + p collisions as obtained from three types of statistics, namely, the Boltzmann (top panels), Tsallis (medium panel), and generic axiomatic statistics (bottom panel). These parameters are the chemical potential μ (left panel), the temperature T (medium panel), and the volume V (right panel). It is found that the chemical potential is approximately inversely proportional to the center-of-mass energies for all particles for the Boltzmann and generic axiomatic statistics; but, by using the Tsallis statistics, there are some variations at low energies. For the Boltzmann and generic axiomatic statistics, the temperature increases with the energies for all particles. For the Tsallis statistics, the temperature decreases with the increase in energies for all particles and their antiparticles except at low energies, the temperature will have a reverse trend. With respect to the volume, we note that the volume in-

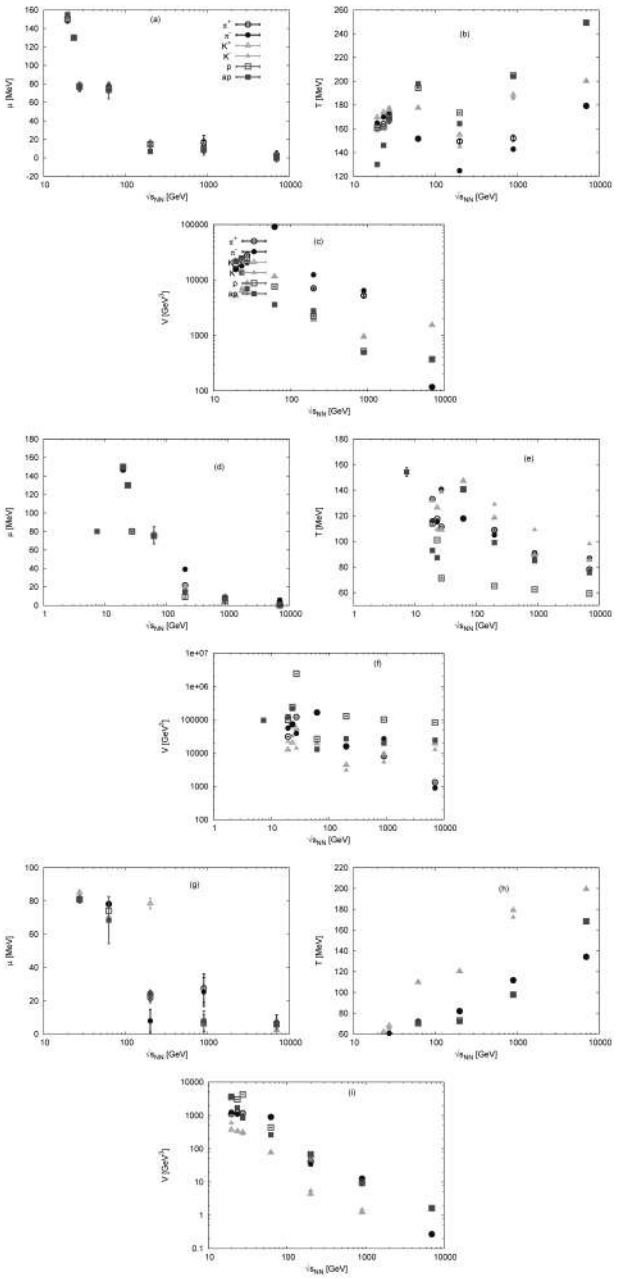

Fig. 4. The various parameters obtained from statistical fits within the Boltzmann, Tsallis, and generic statistics for p_{T} measured in p + p collisions for various charged particles in a wide range of energies, Appendices A.2.a, A.2.b, A.2.c

creases with the energies for all particles using the Boltzmann and generic axiomatic statistics. But the volume decreases with the increase in energies using the Tsallis statistics.

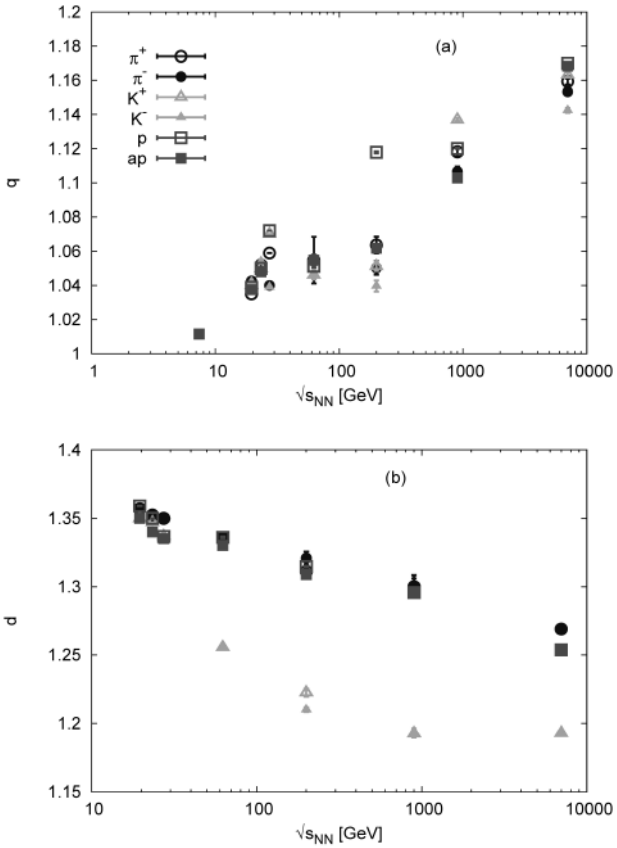

Fig. 5. The nonextensive parameters q and d obtained from statistical fits within the Tsallis and generic axiomatic statistics, respectively, for p_{T} measured in p + p collisions, Appendices A.2.b, A.2.c

Figure 5 shows the nonextensive parameters q and d for the Tsallis and generic axiomatic statistics as functions of the center-of-mass energies for charged particles and antiparticles. In the left panel, we find that q increases with the energies for all particles. On the other hand, d decreases with the increase in the center-of-mass energies for all particles and antiparticles. With this regard, we recall that $c = 0.999506$ for all particles.

Figure 6 shows a comparison of dN/dy and $\langle p_{\mathrm{T}} \rangle$ measured in various experiments in a wide range of energies; UA2 [116], E735 [117], PHENIX [118], STAR [119], ALICE [93] and CMS [95]. It is obvious that the energy dependence for both quantities seems to be consistent with a power-law increase [95].

Figure 7 presents the fit parameters obtained from the three types of statistics as functions of the center-

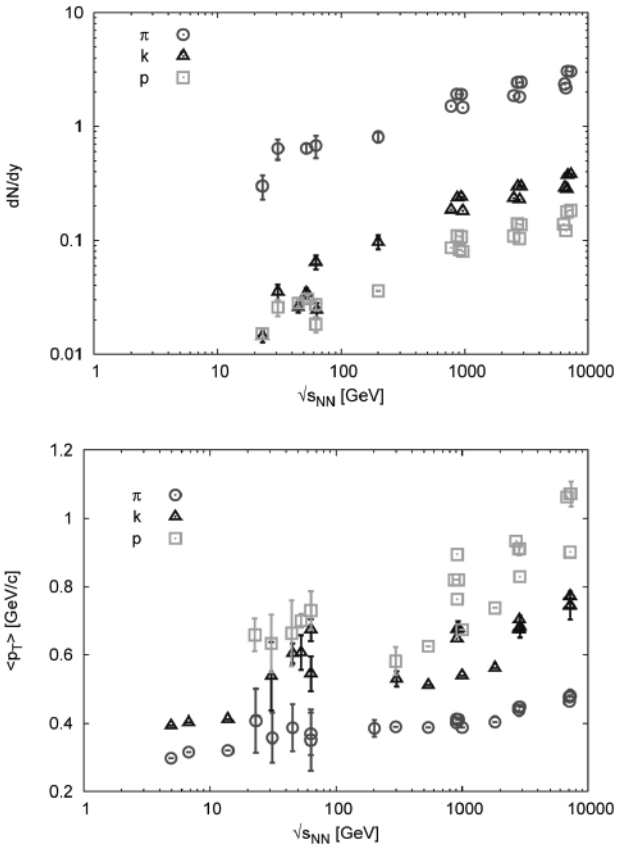

Fig. 6. Left panel shows the central rapidity density dN/dy as a function of $\sqrt{s_{\rm NN}}$ as measured in p + p collisions. The right panel depicts the average transverse momentum $\langle p_{\rm T}\rangle$ as a function of $\sqrt{s_{\rm NN}}$ [92, 95, 109]. Both graphs are taken from Refs. [92, 109]

of-mass energies. The left panel shows a comparison for pions, middle panel illustrates kaons, while the right panel presents protons and antiprotons. The top panel gives the dependence of μ on the center-of-mass energies. An inverse proportionality between μ and the energies is obtained for all particles using all types of statistics. The middle panel shows the temperature as a function of the center-of-mass energies. It is to be noted that, by using the Boltzmann and generic statistics, the temperature increases with the energies for all particles. By using the Tsallis statistics, we find that the temperature decreases with the increase in energies. The bottom panel presents the dependence of the volume on the center-of-mass energies. We find that, by using the Boltzmann and generic statistics, the volume decreases with the increase in energies

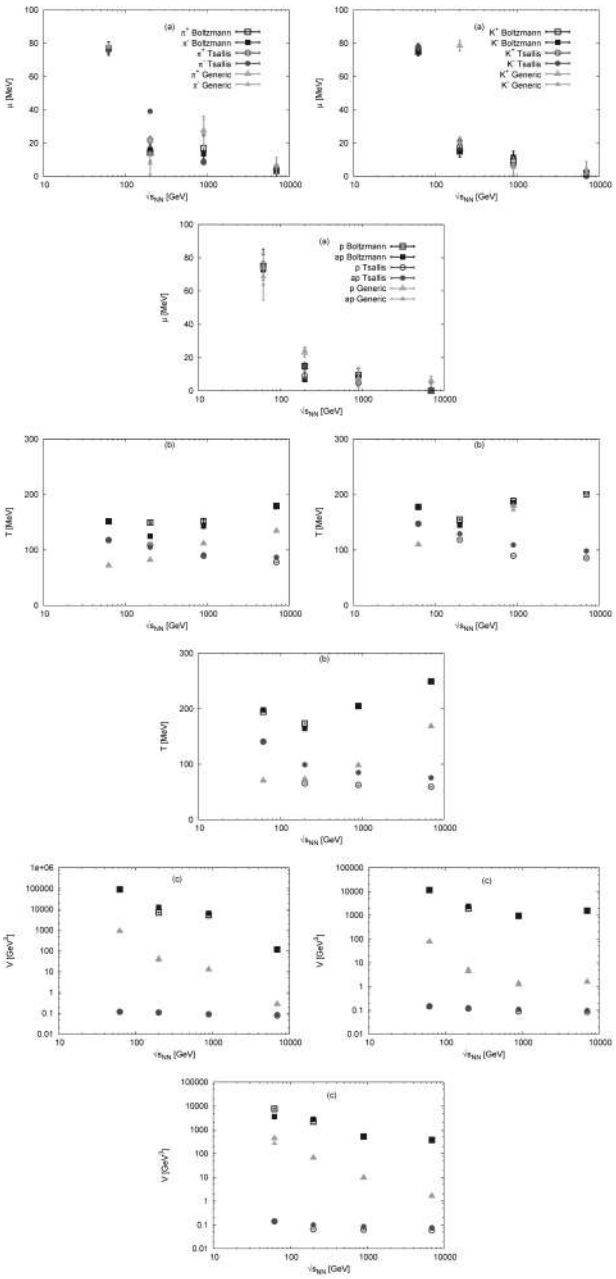

Fig. 7. A comparison between μ, T, and V obtained from statistical fits within the Boltzmann, Tsallis, and generic statistics for $p_{\rm T}$ measured in p + p collisions for various charged particles in a wide range of energies, compare with Fig. 4, Appendices A.2.a, A.2.b, A.2.c

for all particles. By using the Tsallis statistics, the volume is found nearly independent of the increase in the energies.

Table 4 presents results of the statistical fits of the spectra of the combined positive and negative particles measured in p−p collisions at 0.9 GeV with statistical and systematic uncertainties, [93] to Eq. (46). We note that the temperature T and the transverse momentum $p_{\rm T}$ increase with the increase in the particle mass, while the nonextensive parameter n is found nearly independent of the type of particles at 900 GeV. It is approximately in the range between 6 to 8. This means that q ranges between 1.14 and ∼1.2.

For p + p collisions, we conclude that there is a general behavior for the resulting temperature T, namely, T decreases with the increase in energies for all studied particles by using all types of statistics (extensive and nonextensive) except for the Tsallis one, where the temperature increases with the energies at low energies only. For the three types of statistics, the fit parameter μ decreases with the increase in the energies for all particles and antiparticles, but using the Tsallis statistics; there are some variations at low energies. The volume of the system is found to increase with the energies for all particles and their antiparticles by using the Boltzmann and generic statistics. But the obtained V by using the Tsallis statistics are found to have a reverse behavior except the latter. The nonextensive parameter q from the Tsallis statistics increases with the energies for all particles and their antiparticles. In addition, the nonextensive parameter d which is obtained by using the generic statistics, decreases with the increase in the energies for all types of particles.

Table 4. **Results of the statistical fits for the experimental results on the combined positive and negative particles spectra measured in p + p collisions at 0.9 GeV to Eq. (46) [93]. The statistical and systematic uncertainties are indicated**

Particle	dN/dy	T [GeV]	n	$\langle p_{\rm T}\rangle$ [GeV]	χ^2/ndf
$\pi^+ + \pi^-$	$2.977 \pm$	$0.126 \pm$	$7.82 \pm$	$0.404 \pm$	19.69/30
	$\pm 0.007 \pm$	$\pm 0.0005 \pm$	$\pm 0.06 \pm$	$\pm 0.001 \pm$	19.69/30
	± 0.15	± 0.001	± 0.1	± 0.02	19.69/30
$K^+ + K^-$	$0.366 \pm$	$0.160 \pm$	$6.08 \pm$	$0.651 \pm$	8.46/24
	$\pm 0.006 \pm$	$\pm 0.003 \pm$	$\pm 0.2 \pm$	$\pm 0.004 \pm$	8.46/24
	± 0.03	± 0.005	± 0.4	± 0.05	8.46/24
$p + \bar{p}$	$0.162 \pm$	$0.184 \pm$	$7.5 \pm$	$0.764 \pm$	15.70/21
	$\pm 0.003 \pm$	$\pm 0.005 \pm$	$\pm 0.7 \pm$	$\pm 0.005 \pm$	15.70/21
	± 0.012	± 0.007	± 0.9	± 0.07	15.70/21

Table 5. **Results of the statistical fit parameters, q and V, Eq. (11), to the experimental results on particles and antiparticles measured in p + p collisions. The statistical and systematic uncertainties are indicated. The experimental measurements are measured from A + A collisions at energies 7.7, 11.5, 19.6, 27, 39 GeV [61], 62.4 GeV [120]**

$\sqrt{s_{NN}}$, GeV	Particle	q	V, GeV^3
7.7	π^+	1.070 ± 0.006	24646 ± 191.2
	π^-	1.0421 ± 0.0034	28011 ± 330.6
	K^+	1.1556 ± 0.0071	19141 ± 716.4
	K^-	1.1536 ± 0.0035	7634.26 ± 250.5
	p	1.1583 ± 0.0063	205592 ± 5592
	$\bar{p}$	1.1496 ± 0.001	601.35 ± 16.2
11.5	π^+	1.0754 ± 0.0097	68528.5 ± 312.4
	π^-	1.0485 ± 0.0027	90770.5 ± 628.4
	K^+	1.1245 ± 0.0045	50407 ± 1170
	K^-	1.1029 ± 0.0052	24453.4 ± 510.2
	p	1.1298 ± 0.0038	349392 ± 8992
	$\bar{p}$	1.1182 ± 0.0062	3812.81 ± 107.7
19.6	π^+	1.0782 ± 0.0098	288227 ± 1760
	π^-	1.0598 ± 0.01128	276156 ± 2179
	K^+	1.111 ± 0.0074	139986 ± 13736
	K^-	1.0998 ± 0.0026	91402.6 ± 869.1
	p	1.1226 ± 0.0023	406443 ± 7779
	$\bar{p}$	1.0947 ± 0.004	15568.1 ± 341.7
27	π^+	1.0938 ± 0.0032	478484 ± 4488
	π^-	1.0614 ± 0.0043	495359 ± 4169
	K^+	1.0921 ± 0.0019	166034 ± 2944
	K^-	1.091 ± 0.0011	139990 ± 2749
	p	1.1218 ± 0.0024	405526 ± 7991
	$\bar{p}$	1.0849 ± 0.0036	22113.9 ± 462
39	π^+	1.1071 ± 0.0012	924695 ± 7617
	π^-	1.0718 ± 0.0028	775714 ± 62240
	K^+	1.0851 ± 0.0047	200263 ± 2727
	K^-	1.09 ± 0.0011	163264 ± 2749
	p	1.1218 ± 0.0024	322988 ± 6710
	$\bar{p}$	1.0759 ± 0.004	31505.1 ± 776
62.4	π^+	1.1248 ± 0.0136	1736910 ± 46270
	π^-	1.0804 ± 0.0019	1668610 ± 8258
	K^+	1.0795 ± 0.0168	202642 ± 7378
	K^-	1.0894 ± 0.0134	166980 ± 4293
	p	1.1123 ± 0.0047	192694 ± 6284
	$\bar{p}$	1.0732 ± 0.0066	37262.3 ± 1362

Tables 5–8 list all fitting parameters for A + A collisions, at a wide range of energies.

It was concluded that the $p_{\rm T}$ resolution of the CMS experiment does not affect the shape of the measured spectra [94]. For a combination of all (most) charged particles detected in non-single-diffractive $p-p$ collisions, it was found that

• at 0.9 TeV [94], $T = 0.13 \pm 0.01$ GeV, $n = 7.7 \pm \pm 0.2$, $dN_{\rm ch}/dy|_{|y|<0.5} = 3.48 \pm 0.02 \pm 0.13$, and $\langle p_{\rm T}\rangle = 0.46 \pm 0.01 \pm 0.01$ GeV,

• at 2.36 TeV [94], $T = 0.14 \pm 0.01$ GeV, $n = 6.7 \pm \pm 0.2$, $dN_{\rm ch}/dy|_{|y|<0.5} = 4.47 \pm 0.04 \pm 0.16$, and $\langle p_{\rm T}\rangle = 0.50 \pm 0.01 \pm 0.01$ GeV,

• at 7 TeV [95], $T = 0.145 \pm 0.005$ GeV, $n = 6.6 \pm \pm 0.2$, $dN_{\rm ch}/dy|_{|y|<0.5} = 5.78 \pm 0.01 \pm 0.23$, and $\langle p_{\rm T}\rangle = 0.545 \pm 0.005 \pm 0.015$ GeV.

3.1.3. Universal trends of fit parameters

At SPS energies (6.27 and 17.27 GeV), RHIC energies (62.4 and 200 GeV), and LHC energies (0.9, 2.76, and 7 TeV), the charged pion transverse momentum spectra, $p_{\rm T}$, in p + p collisions have been studied as functions of the energy $\sqrt{s}$ and multiplicity by means of the Tsallis nonextensive approach [123]. The Tsallis parameters have been found as functions of the center-of-mass energy $\sqrt{s}$ as in the following expression:

$$f(\sqrt{s}) = (a + (\sqrt{s})^{-\alpha})^b, \tag{64}$$

Table 6. **The same as in Table 5, but at 130 GeV [62], 200 GeV [121], and 2.76 TeV [122]**

$\sqrt{s_{NN}}$, GeV	Particle	q	V, GeV^3
130	π^+	1.1298 ± 0.0094	1660530 ± 28620
	π^-	1.0936 ± 0.0171	877168 ± 34530
	K^+	1.0535 ± 0.0073	114122 ± 3671
	K^-	1.0462 ± 0.0048	70035.9 ± 1364
	p	1.0905 ± 0.001	121031 ± 1372
	$\bar{p}$	1.0667 ± 0.004	24363.9 ± 778.3
200	π^+	1.1391 ± 0.0053	5779680 ± 188900
	π^-	1.1129 ± 0.0023	2844750 ± 49630
	K^+	1.0524 ± 0.002	293292 ± 3430
	K^-	1.0425 ± 0.0018	244108 ± 2075
	p	1.0882 ± 0.0055	104342 ± 5268
	$\bar{p}$	1.0619 ± 0.0056	41584.8 ± 2198
2760	π^+	1.1984 ± 0.0015	15781000 ± 70520
	π^-	1.1538 ± 0.0016	9144990 ± 36320
	K^+	1.052 ± 0.0062	209949 ± 1445
	K^-	1.041 ± 0.0035	200949 ± 1094
	p	1.0877 ± 0.0088	7218.43 ± 75.72
	$\bar{p}$	1.0285 ± 0.0091	5989.29 ± 84.02

Table 7. **Results of the statistical fit parameters, μ, T, Eq. (11), to the experimental results on particles and antiparticles measured in p + p collisions. The statistical and systematic uncertainties are indicated. The experimental measurements are performed for A + A collisions at energies 7.7, 11.5, 19.6, 27, 3 GeV [61], 62.4 GeV [120]**

$\sqrt{s_{NN}}$, GeV	Particle	μ, GeV	T, GeV
7.7	π^+	0.4523 ± 0.0009	0.1349 ± 0.0011
	π^-	0.4389 ± 0.0002	0.14 ± 0.0017
	K^+	0.4481 ± 0.005	0.1191 ± 0.0034
	K^-	0.4484 ± 0.0051	0.1227 ± 0.003
	p	0.4503 ± 0.0054	0.1081 ± 0.0009
	$\bar{p}$	0.4478 ± 0.0064	0.1459 ± 0.0014
11.5	π^+	0.3405 ± 0.002	0.1328 ± 0.0012
	π^-	0.3301 ± 0.0009	0.1347 ± 0.00027
	K^+	0.3354 ± 0.0035	0.121 ± 0.0014
	K^-	0.3361 ± 0.0033	0.1247 ± 0.0012
	p	0.3347 ± 0.0052	0.1104 ± 0.0007
	$\bar{p}$	0.3368 ± 0.0063	0.1506 ± 0.0012
19.6	π^+	0.2175 ± 0.0008	0.124 ± 0.0006
	π^-	0.2093 ± 0.0009	0.1288 ± 0.0007
	K^+	0.2169 ± 0.0022	0.1229 ± 0.0007
	K^-	0.2169 ± 0.0023	0.1272 ± 0.0004
	p	0.2137 ± 0.004	0.1158 ± 0.0005
	$\bar{p}$	0.2201 ± 0.0052	0.1609 ± 0.0009
27	π^+	0.1675 ± 0.0011	0.1154 ± 0.0007
	π^-	0.1605 ± 0.00109	0.125 ± 0.0006
	K^+	0.1665 ± 0.0032	0.1336 ± 0.0008
	K^-	0.1668 ± 0.004	0.1312 ± 0.0009
	p	0.1628 ± 0.0046	0.1231 ± 0.0006
	$\bar{p}$	0.1737 ± 0.0051	0.1697 ± 0.0009
39	π^+	0.1192 ± 0.001	0.1062 ± 0.0004
	π^-	0.12 ± 0.0004	0.1196 ± 0.0002
	K^+	0.1176 ± 0.0021	0.137 ± 0.0006
	K^-	0.1168 ± 0.0037	0.139 ± 0.0008
	p	0.1132 ± 0.0048	0.1289 ± 0.0006
	$\bar{p}$	0.1209 ± 0.0062	0.178 ± 0.0011
62.4	π^+	0.0743 ± 0.0034	0.1054 ± 0.0013
	π^-	0.0787 ± 0.0007	0.1108 ± 0.0002
	K^+	0.0767 ± 0.0067	0.1474 ± 0.0018
	K^-	0.0768 ± 0.0047	0.1504 ± 0.0013
	p	0.0784 ± 0.0075	0.14 ± 0.0011
	$\bar{p}$	0.0781 ± 0.0088	0.1855 ± 0.0017

where $a = 1.33 \pm 0.08$, $\alpha = 0.22 \pm 0.06$ and $b = 4.36 \pm 0.24$ for $n(\sqrt{s})$, $a = 2.63 \pm 0.62$, $\alpha = 0.04 \pm 0.02$ and $b = 3.76 \pm 0.49$ for $T(\sqrt{s})$ and $a = 0.65 \pm 0.01$, $\alpha = 0.22 \pm 0.01$ and $b = -4.78 \pm 0.03$ for $dN(\sqrt{s})/dy$. In addition, the charged pion spectra for different event multiplicities in p + p collisions for LHC energies using the Tsallis distribution was studied [123]. This expression was proposed by fitting the parameters obtained from other fits as functions of the center-of-mass energies. We do the same and add them in the end of this subsection as graphs, expressions, and tables for parameters.

Here, we analyze the transverse momentum spectra $p_{\rm T}$ for charged particles and antiparticles by using extensive and nonextensive statistics. Various fit parameters are obtained from the statistical fits in a wide range of center-of-mass energies by using three types of statistics: the Boltzmann (extensive), Tsallis and generic statistics (nonextensive). We conclude that the Tsallis statistics is more successful in describing p + p collisions than A + A collisions, but MB has the reverse behavior, Sec. 3. The generic statistics is successful in all types of collisions. The Boltzmann statistics can interpret the interaction between many particles, so it can be used excellently with the crowded system (A + A) collisions. But the Tsallis statistics is more accurate to explain the interaction between a finite number of particles; so, it is good in explaining p + p collisions.

Table 8. **The same as in Table 7, but at 130 GeV [62], 200 GeV [121], and 2.76 TeV [122]**

$\sqrt{s_{NN}}$, GeV	Particle	μ, GeV	T, GeV
130	π^+	0.0401 ± 0.0018	0.0815 ± 0.0005
	π^-	0.0445 ± 0.0046	0.1019 ± 0.0017
	K^+	0.04 ± 0.0064	0.1494 ± 0.0014
	K^-	0.0422 ± 0.004	0.1596 ± 0.0009
	p	0.04 ± 0.0025	0.1415 ± 0.0003
	$\bar{p}$	0.0375 ± 0.008	0.1881 ± 0.0013
200	π^+	0.0209 ± 0.0049	0.08 ± 0.0007
	π^-	0.0383 ± 0.0029	0.0993 ± 0.0005
	K^+	0.0176 ± 0.0023	0.1635 ± 0.0005
	K^-	0.0204 ± 0.0019	0.1691 ± 0.0004
	p	0.0084 ± 0.012	0.1522 ± 0.0016
	$\bar{p}$	0.0046 ± 0.0109	0.189 ± 0.0018
2760	π^+	0.0048 ± 0.0008	0.0782 ± 0.0001
	π^-	0.0057 ± 0.0007	0.0969 ± 0.0002
	K^+	0.0003 ± 0.0017	0.2296 ± 0.0006
	K^-	0.0005 ± 0.0017	0.2361 ± 0.0006
	p	0.0027 ± 0.0048	0.3893 ± 0.0018
	$\bar{p}$	0.00013 ± 0.0045	0.4295 ± 0.0024

3.1.4. Our expressions for fitting parameters

The expression for the dependence of μ on the center-of-mass energies for all particles and antiparticles in all statistics at all types of collisions is given as

$$\mu = a\sqrt{s_{\rm NN}}^{b}. \tag{65}$$

a. AA collision. See Figs. 8, 9 and Tables 9, 10, and 11

Table 9. **π^+, π^-, K^+, K^-, p and $\bar{p}$ from A + A collisions with the Boltzmann statistics**

Parameter		π^+	π^-
T	a	366.155	1624.98
	b	0.0256	0.0064
	c	-231.022	-1496.04
μ	a	2285.34 ± 167.5	1999.9 ± 101.3
	b	-0.7854 ± 0.0304	-0.7254 ± 0.0216
V	a	2236.97	3362.76
	b	0.039	0.02696
	c	-2393.4	-3525.18
Parameter		K^+	K^-
T	a	17.6138 ± 16.96	147.906 ± 8.899
	b	0.2437 ± 0.0971	0.0707 ± 0.0124
	c	156.121 ± 25.31	0.0414 ± 4.079
μ	a	2290.63 ± 116.7	2337.01 ± 154.2
	b	-0.7889 ± 0.021	-0.7939 ± 0.0268
V	a	6624.73	780.722
	b	0.0042	0.0293
	c	-6669.49	-824.573
Parameter		p	$\bar{p}$
T	a	169.688 ± 16.74	162.424 ± 11.56
	b	0.1149 ± 0.0251	0.1331 ± 0.0152
	c	0.2419	0.3363
μ	a	2329.17 ± 121.8	2358.88 ± 140
	b	-0.7923 ± 0.0197	-0.7982 ± 0.0227
V	a	240.798	12.0787
	b	-0.02696	0.1953
	c	-190.088	-17.809

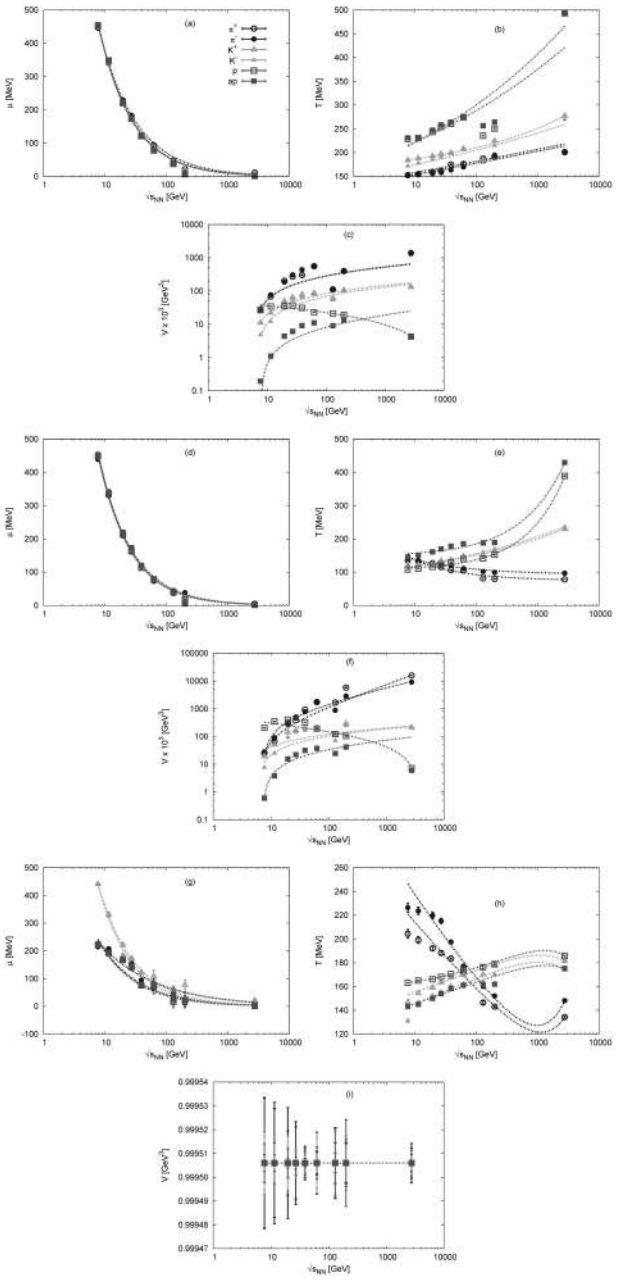

Fig. 8. The various parameters obtained from the statistical fits within the Boltzmann, Tsallis, and generic axiomatic statistics for p_{T} measured in A + A collisions for various charged particles in a wide range of energies

• Volume and temperature using both Boltzmann and Tsallis statistics for all particles

$$V \text{ and } T = a\sqrt{s_{\mathrm{NN}}}^{b} + c. \tag{66}$$

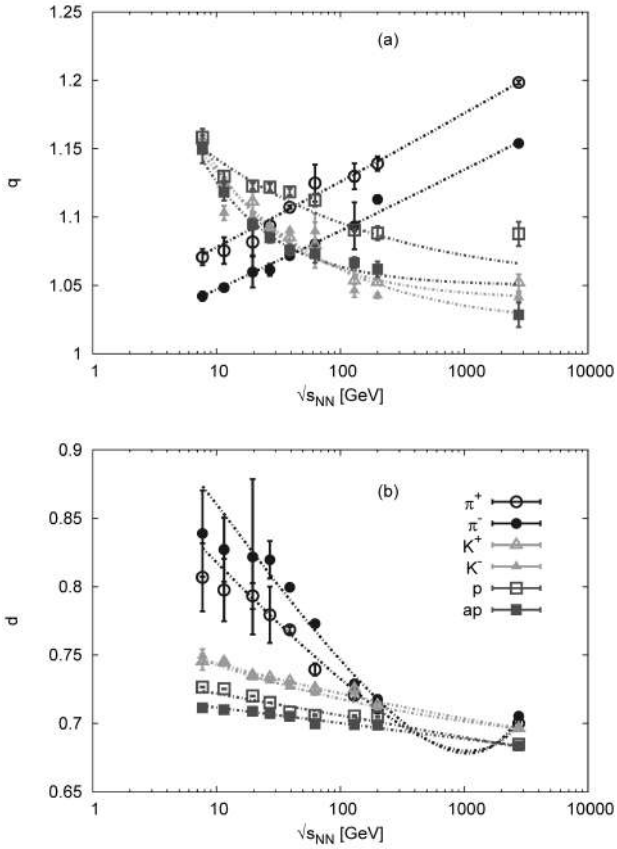

Fig. 9. The nonextensive parameters q and d obtained from statistical fits within the Tsallis and generic axiomatic statistics, respectively, for p_{T} measured in A + A collisions

• q using the Tsallis statistics for all particles except pions

$$q = (a + \sqrt{s_{\mathrm{NN}}}^{b})^{c}. \tag{67}$$

• q using the Tsallis statistics for pions

$$q = a\sqrt{s_{\mathrm{NN}}}^{b}. \tag{68}$$

• Temperature using the generic statistics for all particles

$$T = a\sqrt{s_{\mathrm{NN}}}^{b} + c\sqrt{s_{\mathrm{NN}}} + d. \tag{69}$$

• Volume using the generic statistics for all particles

$$V = (a + \sqrt{s_{\mathrm{NN}}}^{b})^{c}. \tag{70}$$

• d using the generic statistics for all particles

$$d = a\sqrt{s_{\mathrm{NN}}}^{b} + c. \tag{71}$$

b. NN collision. See Figs. 10, 11 and Tables 12, 13, and 14.

• Temperature using the Boltzmann statistics for all particles except π^+

$$T = a\sqrt{s_{\rm NN}}^{b} + c. \tag{72}$$

Table 10. **π^+, π^-, K^+, K^-, p, and $\bar{p}$ from A + A collisions with the Tsallis statistics**

Parameter		π^+	π^-
q	a	1.0321 ± 0.0018	1.0058 ± 0.0027
	b	0.0189 ± 0.0003	0.0174 ± 0.0005
	c		
T	a	221.648 ± 78.34	131.978 ± 24
	b	-0.5487 ± 0.1345	-0.4618 ± 0.0775
	c	74.8777 ± 2.951	93.1116 ± 2.6
μ	a	2335.51 ± 67.11	2423.89 ± 70.4
	b	-0.8018 ± 0.0117	-0.8215 ± 0.0096
V	a	36.5323	188.568
	b	0.771 ± 0.0642	0.504 ± 0.0669
	c	-155.883 ± 55.11	-510.2 ± 155.2
Parameter		K^+	K^-
q	a	1.0849 ± 0.0087	1.0575 ± 0.0494
	b	0.6513 ± 0.0778	0.4631 ± 0.1519
	c	0.4776 ± 0.0682	0.3704 ± 0.0894
T	a	41.1363 ± 15.58	62.3076 ± 13.8
	b	0.1819 ± 0.0333	0.1507 ± 0.0179
	c	55.6623 ± 20.74	30.5037 ± 16.89
μ	a	2558.91 ± 188.6	2597.82 ± 189.6
	b	-0.8372 ± 0.0268	-0.8427 ± 0.0273
V	a	4872.6	4868.99
	b	0.0068 ± 0.3914	0.0072 ± 0.2531
	c	-4908	-4928.96
Parameter		p	$\bar{p}$
q	a	1.2096 ± 0.1506	1.1079 ± 0.0274
	b	-0.337 ± 0.216	-0.7548 ± 0.1805
	c	0.2601 ± 0.0391	0.4746 ± 0.1564
T	a	1.268 ± 0.4772	2.1977 ± 1.697
	b	0.6814 ± 0.0478	0.6115 ± 0.0955
	c	107.78 ± 3.91	148.16 ± 8.675
μ	a	2525.43 ± 109.1	2309.37 ± 153.5
	b	-0.8368 ± 0.0167	-0.7958 ± 0.026
V	a	710.35	68.9332
	b	-0.1682 ± 0.1836	0.1231 ± 0.3134
	c	-180.231 ± 283.4	-88.0645 ± 250.6

• Temperature using the Boltzmann statistics for π^+

$$T = (a + \sqrt{s_{\rm NN}}^{b})^{c}. \tag{73}$$

Table 11. **π^+, π^-, K^+, K^-, p and $\bar{p}$ from A + A collisions with the generic statistics**

Parameter		π^+	π^-
d	a	1.0823 ± 0.4478	2.0036 ± 1.156
	b	-0.7764 ± 0.1178	-0.8307 ± 0.158
	c	0.6961 ± 0.0036	0.6987 ± 0.0065
T	a	1453.05	733.242 ± 2.352
	b	-0.0184 ± 0.2311	-0.0512 ± 0.2068
	c	0.0206 ± 0.0155	0.0267 ± 0.0157
	d	-1178.5	-414.133 ± 2.410
μ	a	1051.61 ± 171	920.591 ± 211
	b	-0.72 ± 0.0512	-0.6621 ± 0.0872
V	a	1.0944 ± 0.0978	1.0843 ± 0.0427
	b	-3.32×10^{-11}	-1.18×10^{-11}
	c	-6.68×10^{-4}	-6.73×10^{-4}
Parameter		K^+	K^-
d	a	0.1595 ± 0.0803	0.1111 ± 0.005
	b	-0.0781 ± 0.069	-0.1814 ± 0.075
	c	0.6106 ± 0.0903	0.6698 ± 0.0164
T	a	507.074	572.39
	b	0.0156 ± 0.3464	0.0158 ± 0.4227
	c	-0.008 ± 0.0106	-0.0099 ± 0.0146
	d	-370.448	-448.213
μ	a	2038.82 ± 102.7	2359.56 ± 210
	b	-0.7502 ± 0.0212	-0.8202 ± 0.0393
V	a	0.3676	0.3676
	b	-8.2487 ± 0.2022	-8.5591 ± 0.2022
	c	4.94×10^{-4}	4.94×10^{-4}
Parameter		p	$\bar{p}$
d	a	3.0078	1.7382
	b	0.0023	-0.0029
	c	3.7456	-1.015
T	a	6.43045 ± 7.528	644.49
	b	0.3024 ± 0.1859	0.0121 ± 0.277
	c	-0.0131 ± 0.0116	-0.0061 ± 0.0098
	d	151.206 ± 9.971	-517.177
μ	a	625.662 ± 139.4	605.863 ± 111.5
	b	-0.4797 ± 0.0817	-0.466 ± 0.0674
V	a	3.6721	3.5195
	b	-7.2576	-7.1715
	c	-3.8×10^{-4}	-3.93×10^{-4}

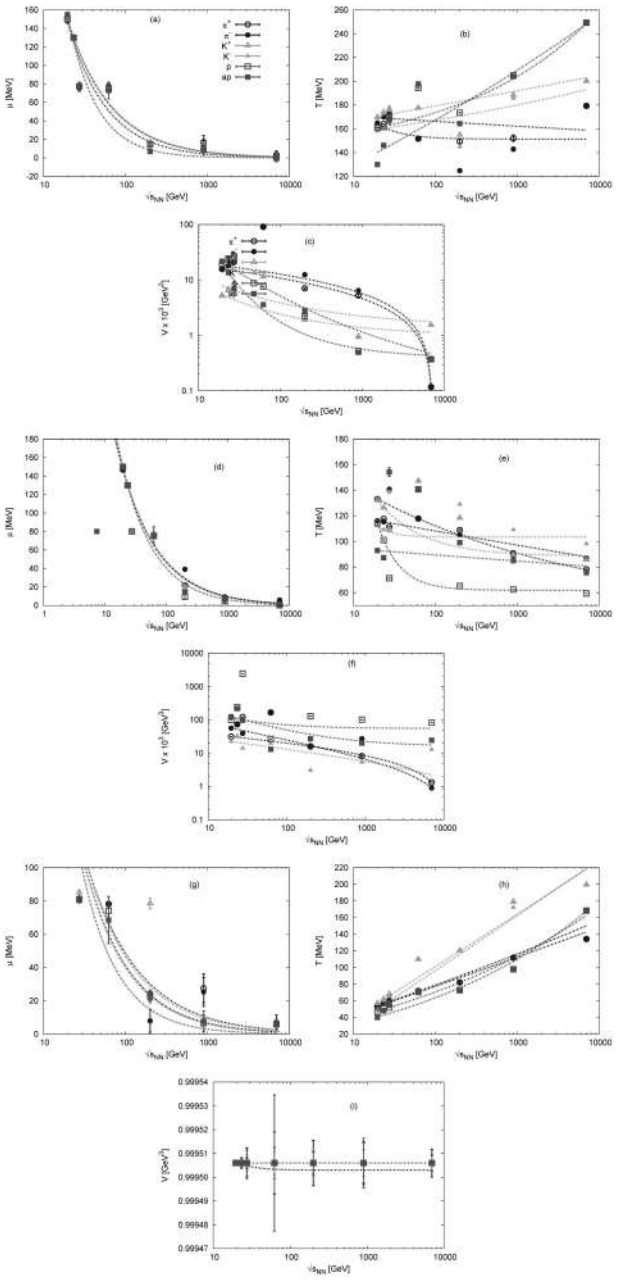

Fig. 10. The various parameters obtained from the statistical fits within the Boltzmann, Tsallis, and generic axiomatic statistics for p_{T} measured in NN collisions for various charged particles in a wide range of energies

• Volume using the Boltzmann statistics for all particles except pions

$$V = (a + \sqrt{s_{\mathrm{NN}}}^{b})^{c}. \tag{74}$$

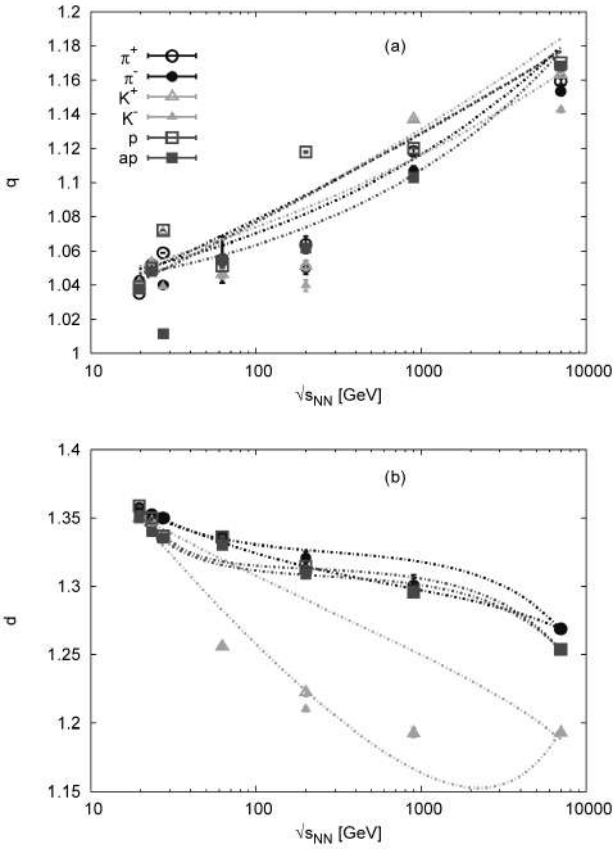

Fig. 11. The nonextensive parameters q and d obtained from statistical fits within the Tsallis and generic axiomatic statistics, respectively, for p_{T} measured in NN collisions

• Volume using the Boltzmann statistics for pions

$$V = a\sqrt{s_{\mathrm{NN}}}^{b} + c. \tag{75}$$

• Temperature and Volume using the Tsallis statistics for all particles

$$T \text{ and } V = a\sqrt{s_{\mathrm{NN}}}^{b} + c. \tag{76}$$

• q using the Tsallis statistics for all particles

$$q = a\sqrt{s_{\mathrm{NN}}}^{b} + c. \tag{77}$$

• Temperature using the generic statistics for all particles

$$T = a\sqrt{s_{\mathrm{NN}}}^{b} + c. \tag{78}$$

• Volume using the generic statistics for all particles

$$V = (a + \sqrt{s_{\mathrm{NN}}}^{b})^{c}. \tag{79}$$

• d using the generic statistics for all particles

$$d = a\sqrt{s_{\rm NN}}^{b} + c\sqrt{s_{\rm NN}} + d. \quad (80)$$

3.2. Empirical parametrization

The transverse momentum spectra of the charged particles produced in A + A collisions at STAR experiment are wel ldescribed in Refs. [61, 62] by using different parametrizations at low p_T ranges. These parametrizations are known as the Bose–Einstein, m_T-exponential, double-exponential, Boltzmann, p_T-exponential, p_T-Gaussian, and p_T^3-exponential. Each of these expressions suggests different power-scales which are compared with the Tsallis statistics at various ranges of p_T at a wide range of energies [62,63]. It was noticed that the temperatures T of the p_T spectra of pions are smaller than that of the kaons, which, in turn, are smaller than that of the protons, and there

Table 12. **π^+, π^-, K^+, K^-, p and $\bar{p}$ in NN collisions with the Boltzmann statistics**

Parameter		π^+	π^-
T	a	1.6857	88.2315
	b	-1.4192 ± 0.8944	-0.0231
	c	9.5912	86.9598
μ	a	1653.35 ± 107.1	2264.02 ± 1346
	b	-0.8062 ± 0.0218	-0.9173 ± 0.1988
V	a	58.7295	110.746
	b	-0.0669	-0.0336
	c	-32.3597	-82.102
Parameter		K^+	K^-
T	a	403.785	40.296
	b	0.0127	0.0845
	c	-248.923	107.799
μ	a	1660.09 ± 15.36	1604.13 ± 648.1
	b	-0.8079 ± 0.0031	-0.797 ± 0.1283
V	a	0.9858 ± 0.2958	0.975 ± 0.3719
	b	-0.4233	-0.3495
	c	6.8653	5.9862
Parameter		p	$\bar{p}$
T	a	10.9573	290.24
	b	0.2623 ± 0.1956	0.0476
	c	136.919 ± 33.44	-194.298
μ	a	1693.96 ± 7.738	6210.22 ± 2995
	b	-0.8143 ± 0.0015	-1.24029 ± 0.1623
V	a	0.77719 ± 0.2041	0.9643 ± 0.0393
	b	-0.2149 ± 0.1369	-0.6189 ± 0.2454
	c	11.1992 ± 0.7657	25.8099 ± 16.88

Table 13. **π^+, π^-, K^+, K^-, p and $\bar{p}$ in NN collisons with the Tsallis statistics**

Parameter		π^+	π^-
q	a	0.2541 ± 0.4988	0.0207 ± 0.0319
	b	0.0589 ± 0.0857	0.2247 ± 0.1415
	c	0.7323 ± 0.5171	1.0023 ± 0.0453
T	a	145.732 ± 9.79	544.518 ± 29.89
	b	-0.1596 ± 0.0618	-0.0093 ± 0.0535
	c	42.4196 ± 22.44	-413.4 ± 2992
μ	a	1157.72 ± 14.3	1212.68 ± 1.873
	b	-0.6936 ± 0.004	-0.7083 ± 0.0005
V	a	78.8988 ± 22.24	240.609 ± 109.8
	b	-0.1607 ± 0.3684	-0.4709 ± 0.1771
	c	-17.6903 ± 67.37	-2.8175 ± 4.21
Parameter		p	$\bar{p}$
q	a	0.2482 ± 1.042	0.0553 ± 0.0964
	b	0.0648 ± 0.2006	0.1362 ± 0.1329
	c	0.7391 ± 1.084	0.959 ± 0.1118
T	a	460.555 ± 123	13630.3 ± 9926
	b	-0.792 ± 0.1478	-2.4715 ± 2.747
	c	88.5391 ± 7.546	103.443 ± 7.619
μ	a	1658.21 ± 3.972	1658.21 ± 4.229
	b	-0.8075 ± 0.0008	-0.8075 ± 0.0008
V	a	18.0347 ± 91.2	58.2233 ± 48.84
	b	-0.3884 ± 2.899	-0.2917 ± 0.776
	c	7.0449 ± 21.16	-2.1949 ± 37.23
Parameter		p	$\bar{p}$
q	a	0.4962 ± 2.562	0.0112 ± 0.0042
	b	0.0368 ± 0.1573	0.2983 ± 0.038
	c	0.4854 ± 2.599	1.0103 ± 0.0072
T	a	7144.68 ± 4531	195.214 ± 1756
	b	-1.6503 ± 0.2559	-0.0113 ± 1.087
	c	61.8312 ± 6.817	-95.8192 ± 1758
μ	a	1658.69 ± 23.16	1658.17 ± 4.187
	b	-0.8076 ± 0.0046	-0.8075 ± 0.0008
V	a	507.172 ± 3511	904.151 ± 855.8
	b	-0.8035 ± 2.623	-0.7149 ± 0.348
	c	53.8495 ± 58.24	15.9831 ± 12.73

Table 14. **π^+, π^-, K^+, K^-, p, and $\bar{p}$ from NN collisions in the generic statistics**

Parameter		π^+	π^-	K^+	K^-	p	$\bar{p}$
d	a	0.205 ± 0.0153	0.7467 ± 0.4243	0.6785	0.8667	17.0142	3.3009 ± 1.629
	b	-0.316 ± 0.1682	-1.0578 ± 0.2557	-0.0459	-0.0952	-1.9958 ± 0.811	-1.4706 ± 0.1815
	c	-2.92×10^{-6}	-8.15×10^{-6}	-3.18×10^{-6}	1.78×10^{-5}	-8.72×10^{-6}	-7.86×10^{-6}
	d	1.2768 ± 0.0382	1.3257 ± 0.0064	0.7589	0.6968	1.3144 ± 0.0124	1.3086 ± 0.0027
T	a	383.23	1202.9	2979.56	2764.39	57.9144	38.0148
	b	0.0347	0.0118	0.0087	0.0098	0.1419 ± 0.071	0.1826 ± 0.1286
	c	-370.846	-1194	-3000.95	-2796.3	-40.8008	-25.3469
μ	a	1576.51 ± 774.6	1155.98 ± 294.4	1268.41 ± 495.8	1685.21 ± 1106	2911.71 ± 1637	2911.71 ± 1637
	b	-0.792 ± 0.1579	-0.6887 ± 0.0836	-0.7179 ± 0.1288	-0.8132 ± 0.2202	0.9965 ± 0.188	-0.9965 ± 0.188
V	a	0.7906	3.9914	0.3676	1.0554 ± 0.3445	3.4952	3.6782
	b	-2.1688	-4.7909	-5.7383 ± 0.9463	6.26×10^{-11}	-5.2047	-5.3507
	c	0.0021	-0.00036	0.00049	-0.00069	-0.00039	-0.00038

is a linear dependence of T on the energies except for protons and antiprotons at 19.6 GeV or 27 GeV, where a rapid increase or decrease is found. It was concluded that the temperature of charged particles are slightly greater than the ones for the antiparticles.

The high transverse momentum p_T spectra of hadrons produced in AA collisions at the top of RHIC energies [65] are found strongly suppressed by a factor of 4–5 [66–71] comparing to the results for the same hadrons in p + p collisions at the same energies [69, 72–75]. Different parametrization have been used to describe the p_T spectra at LHC energies [90, 92–96].

The Tsallis statistics is more effective within the low p_T range rather than in the high p_T. We conclude that the Tsallis statistics is remarkably successful in describing p + p collisions rather than AA collisions. The results obtained from these parametrizations are given in Tables 1–3.

3.3. Other models for p_T spectral distributions

Different parametrizations as the Tsallis–Pareto, Tsallis–Levy [97], and multicomponent Erlang p_T spectral distribution have been proposed to analyze the transverse momentum spectra in various collisions at different centralities [58, 102] in order to determine the effective temperature of the interacting system.

By using two types of Tsallis approaches, e.g., with and without thermodynamic description, the energy dependences of the transverse momentum spectra for charged particles in p + p collisions were analyzed [32]. The obtained temperatures from the thermodynamic description are noted to be smaller than the ones without such description.

The discrepancies of the temperatures using the Tsallis distribution with thermodynamical description is related to the addition of the extra term m_T in the distribution. The effect of the choice of E_T in the Tsallis distribution beats the effect of the extra term m_T for the heavier particles.

Type-A Tsallis distribution was given in Ref. [32] as

$$\left(E\frac{d^3N}{dp^3}\right)_{|\eta|<a} = A\left(1+\frac{E_T}{nT_5}\right)^{-n}, \tag{81}$$

where $E_T = m_T - m$. A, n and T are free fitting parameters. If the self-consistent thermodynamical description was considered, then the Tsallis distribution at the midrapidity would be

$$E\frac{d^3N}{dp^3} = gV\frac{m_T}{(2\pi)^3}\left[1+(q-1)\frac{m_T}{T_1}\right]^{-q/(q-1)}. \tag{82}$$

where g is defined as the degeneracy of the particle, and V is the volume. The previous equation is known as Type-B Tsallis distribution which was very similar to Eq. (81), but m_T was replaced by E_T, and also there was an extra term m_T in front of the bracket [32]. There are three stages or transitions between the two types of the Tsallis distribution (A and B). The first one is known as a Tsallis-like distribution which was obtained in the scope of nonextensive statistics for the particle yield at the midrapidity as given in

Table 15. **The fitting parameter T and corresponding χ^2/ndf in the distributions, Eqs. (82, 83, 84, 85, 81), for the particle spectra in p + p collisions. The unit of T is GeV. Taken from Ref. [32]**

Experiment	$\sqrt{s}$ (GeV)	Particle	T_1	χ^2_1/ndf	T_2	χ^2_2/ndf	T_3	χ^2_3/ndf	T_4	χ^2_4/ndf	T_5	χ^2_5/ndf
PHENIX [118]	62.4	π^+	0.0927	6.857/23	0.085	6.866/23	0.133	4.767/23	0.123	4.784/23	0.132	4.779/23
		π^-	0.0898	8.049/23	0.0824	8.045/23	0.128	5.173/23	0.118	5.198/23	0.130	5.194/23
		K^+	0.0856	4.837/13	0.0775	4.822/13	0.122	5.141/13	0.105	5.349/13	0.160	5.121/13
		K^-	0.0936	2.002/13	0.0851	2.006/13	0.130	2.199/13	0.119	2.203/13	0.163	2.186/13
		p	0.106	7.017/ 24	0.101	7.075/24	0.133	6.934/24	0.125	6.945/24	0.179	6.966/24
		$\bar{p}$	0.0635	6.605/22	0.0588	6.563/22	0.0831	6.037/22	0.0817	5.079/22	0.148	7.178/22
PHENIX [118]	200	π^+	0.0741	5.278/24	0.0657	5.275/24	0.111	4.491/24	0.0981	4.515/24	0.114	4.485/24
		π^-	0.0811	4.710/24	0.0725	4.703/24	0.121	3.350/24	0.108	3.372/24	0.123	3.354/24
		K^+	0.0473	1.561/13	0.0418	1.591/13	0.0729	1.634/13	0.0601	1.602/13	0.138	1.587/13
		K^-	0.0621	3.013/13	0.0542	3.010/13	0.0913	3.004/13	0.0781	2.999/13	0.147	2.999/13
		p	0.0311	23.832/31	0.0279	23.659/31	0.0404	24.004/31	0.0350	24.272/31	0.145	24.581/31
		$\bar{p}$	0.0473	12.902/31	0.0426	12.970/31	0.0609	13.240/31	0.0547	13.153/31	0.154	13.535/31
STAR [125]	200	π^+	0.0895	6.545/20	0.0809	6.539/20	0.126	5.032/20	0.113	5.008/20	0.128	5.009/20
		π^-	0.0900	6.855/20	0.0814	6.854/20	0.127	4.700/20	0.114	4.718/20	0.128	4.705/20
		p	0.0804	10.683/17	0.0735	10.653/17	0.104	10.375/17	0.0950	10.396	0.180	10.359/17
		$\bar{p}$	0.0765	10.380/17	0.0695	10.318/17	0.0995	10.079/17	0.0901	10.076/17	0.177	9.991/17
ALICE [93]	900	π^+	0.0716	24.640/30	0.0627	25.530/30	0.123	13.528/30	0.107	13.749/30	0.125	13.460/30
		π^-	0.0727	17.138/30	0.0636	17.602/30	0.125	12.394/30	0.109	12.645/30	0.126	12.483/30
		K^+	0.0568	12.790/24	0.0488	12.807/24	0.0904	13.034/24	0.0749	13.069/24	0.159	12.980/24
		K^-	0.0624	6.457/24	0.0538	6.552/24	0.0968	6.641/24	0.0820	6.636/24	0.161	6.609/24
		p	0.0397	13.879/21	0.0358	13.908/21	0.0522	13.816/21	0.0460	13.849/21	0.175	13.974/21
		$\bar{p}$	0.0649	13.586/21	0.0568	13.674/21	0.119	14.860/21	0.0769	13.544/21	0.188	13.675/21

Ref. [124]

$$E\frac{d^3N}{dp^3} = Am_T\left[1+(q-1)\frac{m_T}{T_2}\right]^{-\frac{1}{q-1}}, \tag{83}$$

where A, q and T are fitting parameters. Comparing Eq. (83) and Eq. (82), the only difference is the power of the distribution function, i.e., q for Eq. (82) and 1 for Eq. (83). The second form of the distribution is [32]

$$E\frac{d^3N}{dp^3} = A\left[1+(q-1)\frac{m_T}{T_3}\right]^{-\frac{q}{q-1}}, \tag{84}$$

where the term m_T outside of the bracket in Eq. (82) was neglected, and the constants are absorbed into the parameter A [32]. The third one is

$$E\frac{d^3N}{dp^3} = A\left[1+(q-1)\frac{m_T}{T_4}\right]^{-\frac{1}{q-1}}. \tag{85}$$

From Table 15, it is seen that all distributions have the same fitting goodness to the particle spectra. Temperatures of Type-A Tsallis distribution and Type-B Tsallis one are known as T_5 and T_1, respectively. While, T_2, T_3 and T_4 are deduced from the transitions between both types, A and B, of the Tsallis distribution. The Type-A Tsallis distribution gives higher T than the Type-A Tsallis distribution. For all the particles, the temperatures T_1 and T_2 from the distributions with extra m_T term are lower than the temperatures T_3, T_4 and T_5 from the distributions without it. In addition, it was found that T_1 is larger than T_2, the parameter q in Eq. (82) leads to larger T. Similarly, T_4 is smaller than T_5, the m_T in Eq. (85) leads to a smaller temperature. Finally, the temperatures T_3 and T_5 for pions are similar, which results from cancelling the effects of q and m_T on each other. But, for kaons and protons, the effect of m_T in Eq. (84) overcomes the effect of q, so T_3 was smaller than T_5.

4. Conclusions

The transverse momentum spectra p_{T} for the charged particles and antiparticles at a wide range of center-of-mass energies from various high-energy collisions are studied. Extensive and nonextensive statistics were used to analyze the p_{T} spectra for charged particles. The p_{T} spectra for kaons, pions, and protons and their antiparticles are well reproduced by using the Maxwell–Boltzmann, Tsallis, and generic axiomatic statistics. Different fit parameters are estimated for each particle by using the three types of statistics for $\mathrm{A}+\mathrm{A}$ and $\mathrm{p}+\mathrm{p}$ collisions. Specifically, for $\mathrm{p}+\mathrm{p}$ collisions, there is a general trend for the temperature T, namely, T increases with the energies by using all types of statistics (extensive and nonextensive) for all particles except pions, where the temperature decreases with the increase in the energies for the nonextensive statistics, only. We also noticed that the values of T for antiparticles are slightly greater than the ones from the particles. For the three types of statistics, the fit parameter μ decreases with the increase in the energies for all particles and antiparticles. The volume of the system is found decreasing with the increase in energies for all particles and their antiparticles by using the Boltzmann and generic axiomatic statistics. But the values V obtained by using the Tsallis statistics are found nearly independent of changes in the energies for protons and kaons and their antiparticles, while decrease slightly for pions. The nonextensive parameter q from the Tsallis statistics increases with the energies for all particles and their antiparticles except at energies of 62.4 and 200 GeV. In addition, the nonextensive parameter d which is obtained by using the generic axiomatic statistics decreases with the increase in the energies for all types of particles.

But, for $\mathrm{A}+\mathrm{A}$ collisions, it was noticed that, by using the Boltzmann statistics, there is a general behavior that the temperature increases with the energies for all particles. At 200 GeV, the temperature becomes smaller than the ones at lower energies. In addition, we conclude that the temperature obtained for antiparticles are slightly greater than the ones for particles. But, for a nonextensive statistics, the temperature increases with the energies for all particles except for pions. Another exception for pions could be highlighted that there is a reverse proportionality between the temperature and the energies. The resulting temperature from p_{T} spectra of antipions, antikaons, and antiprotons are slightly greater than that from p_{T} spectra of their particles.

Using various parametrization expressions, it was noted that the Tsallis statistics is more effective within the low p_T range, rather than in the high p_T. We conclude that the Tsallis statistics is remarkably successful in describing $\mathrm{p}+\mathrm{p}$ collisions, rather than $\mathrm{A}+\mathrm{A}$ collisions.

We conclude that the generic axiomatic statistics is well applicable in describing both types of collisions at all energies for charged particles and their antiparticles. While the Tsallis statistics is more successful in describing $\mathrm{p}+\mathrm{p}$ collisions, rather than $\mathrm{A}+\mathrm{A}$ collisions, with the Boltzmann statistics describes well the latter more than the former.

The values obtained for the equivalent classes (c, d) that $c \to 1$, while $0 < d < 1$ warrens the conclusion that the resulting Lambert-W exponentials characterize entropic equivalence classes. This means that the fractional-power law and the entropy of the system of interest are characterized by delayed relaxation.

APPENDIX A.
Statistical-thermal approaches

1. A + A collisions

a. Maxwell–Boltzmann statistical fits. Figure 12 presents the analysis for the transverse momentum spectra p_{T} for charged particles and their antiparticles at energies ranging from 7.7 GeV to 2.76 TeV by using the Maxwell–Boltzmann statistics. The experimental results measured in $\mathrm{A}+\mathrm{A}$ collisions are represented by symbols. Open symbols refer to the charged particles, while the closed symbols refer to the antiparticles. The spectra fitted by using the Maxwell–Boltzmann statistics are depicted by curves. It is found that the Maxwell–Boltzmann statistics fits well the transverse momentum distributions for all particles. The fit parameters are compared to those obtained from different statistics for all particles at the whole range of energies, Fig. 3.

b. Tsallis statistical fits. Figure 13 shows the statistical analysis of the transverse momentum spectra p_{T} of charged particles and their antiparticles by using the Tsallis statistics (curves) at energies ranging from 7.7 GeV to 2.76 TeV. The experimental results from $\mathrm{A}+\mathrm{A}$ collisions are given by symbols. The open symbols refer to the charged particles, while the closed ones refer to antiparticles. It is obvious that the Tsallis statistics fits well all studied particles. The fit parameters are compared to those obtained from different types of statistics

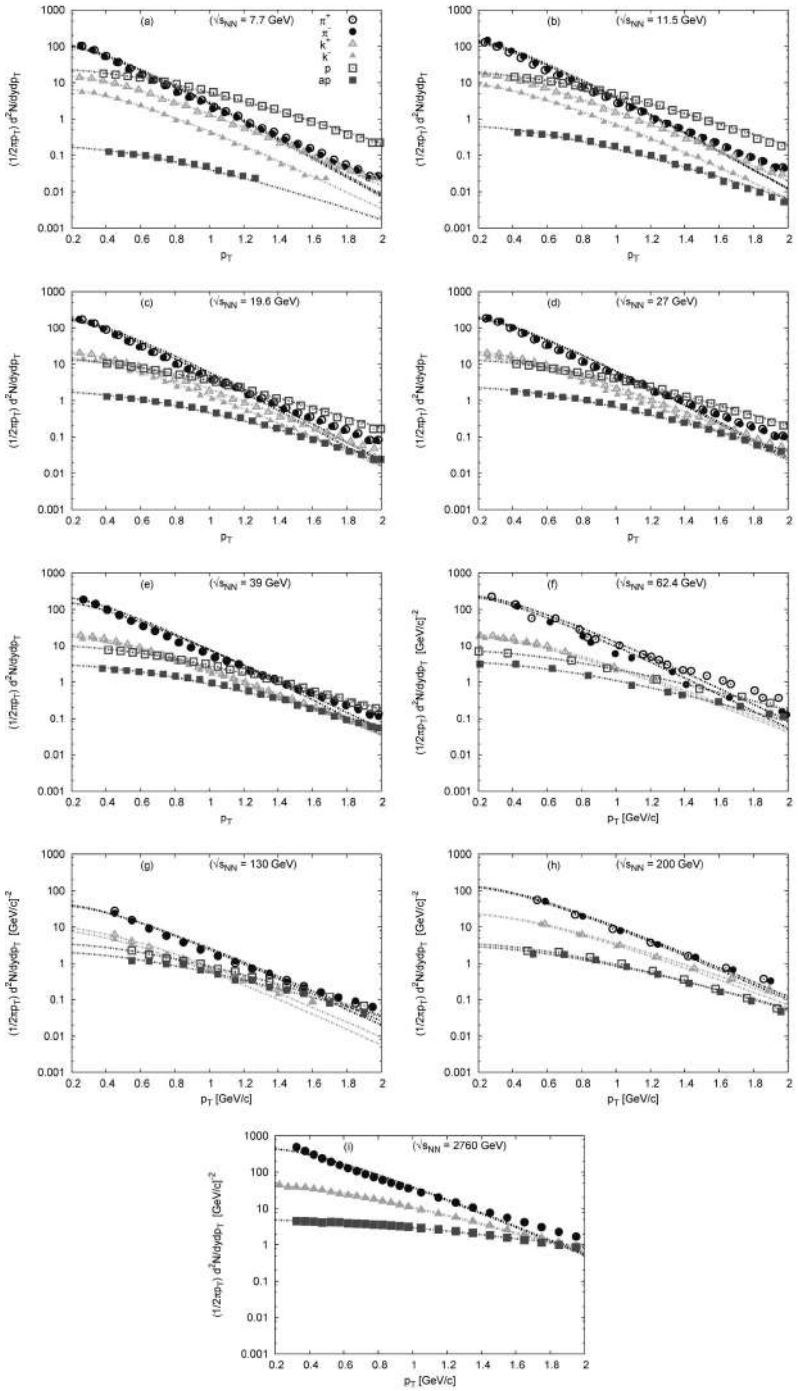

Fig. 12. The transverse momentum spectra p_{T} for charged particles measured from A + A collisions in a wide range of energies are analyzed by using the Maxwell–Boltzmann statistics. Panels (a)–(i) refer to the change in the center-of-mass energies from 7.7 to 11.5 to 19.6 to 27 to 39 to 62.4 to 130 to 200 GeV and to 2.76 TeV, respectively. The fit parameters are shown in Fig. 3

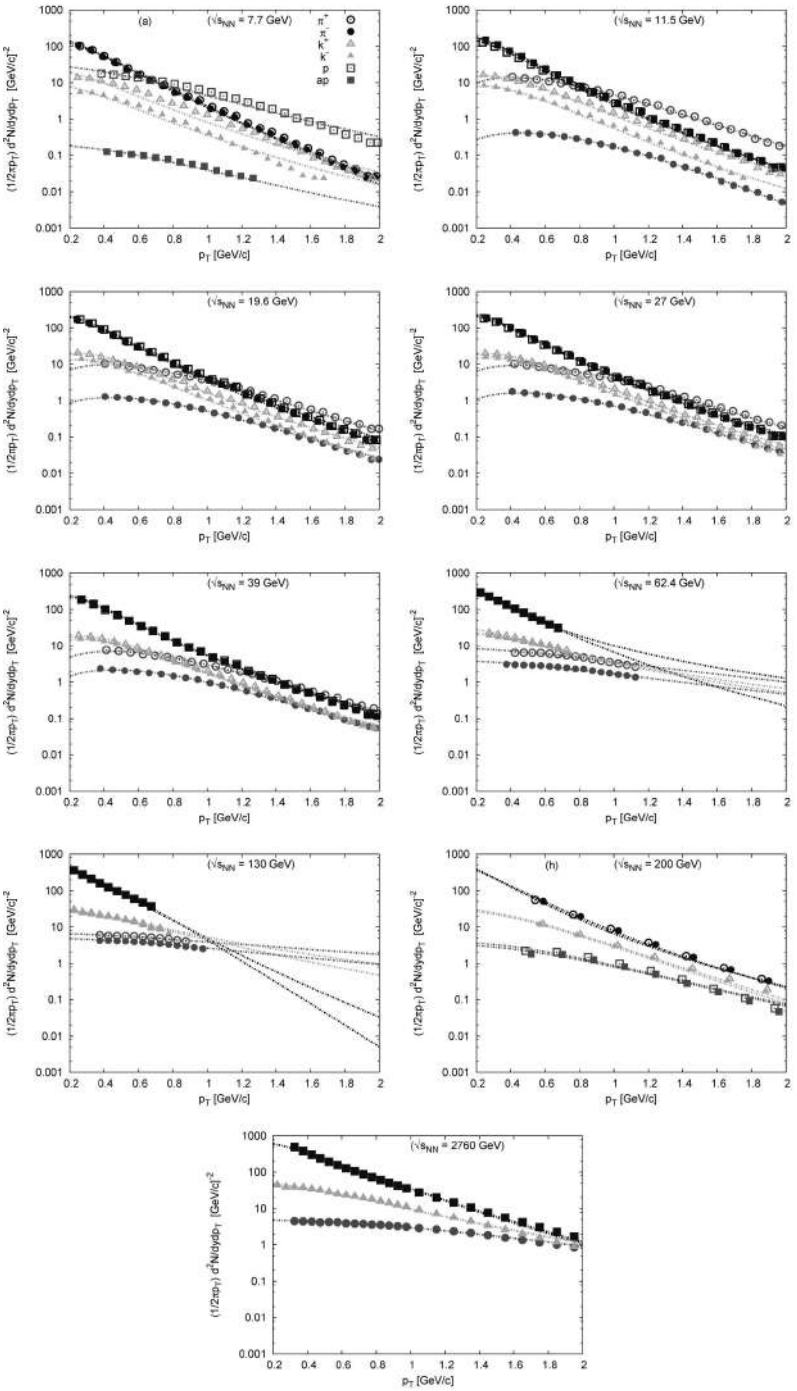

Fig. 13. The transverse momentum spectra p_{T} for charged particles measured from A + A collisions at a wide range of energies are fitted to the Tsallis statistics. Panels (a)–(i) show the impacts of changing energies from 7.7 to 11.5 to 19.6 to 27 to 39 to 62.4 to 130 to 200 GeV and to 2.76 TeV, respectively. The corresponding fit parameters are illustrated in Figs. 2 and 3

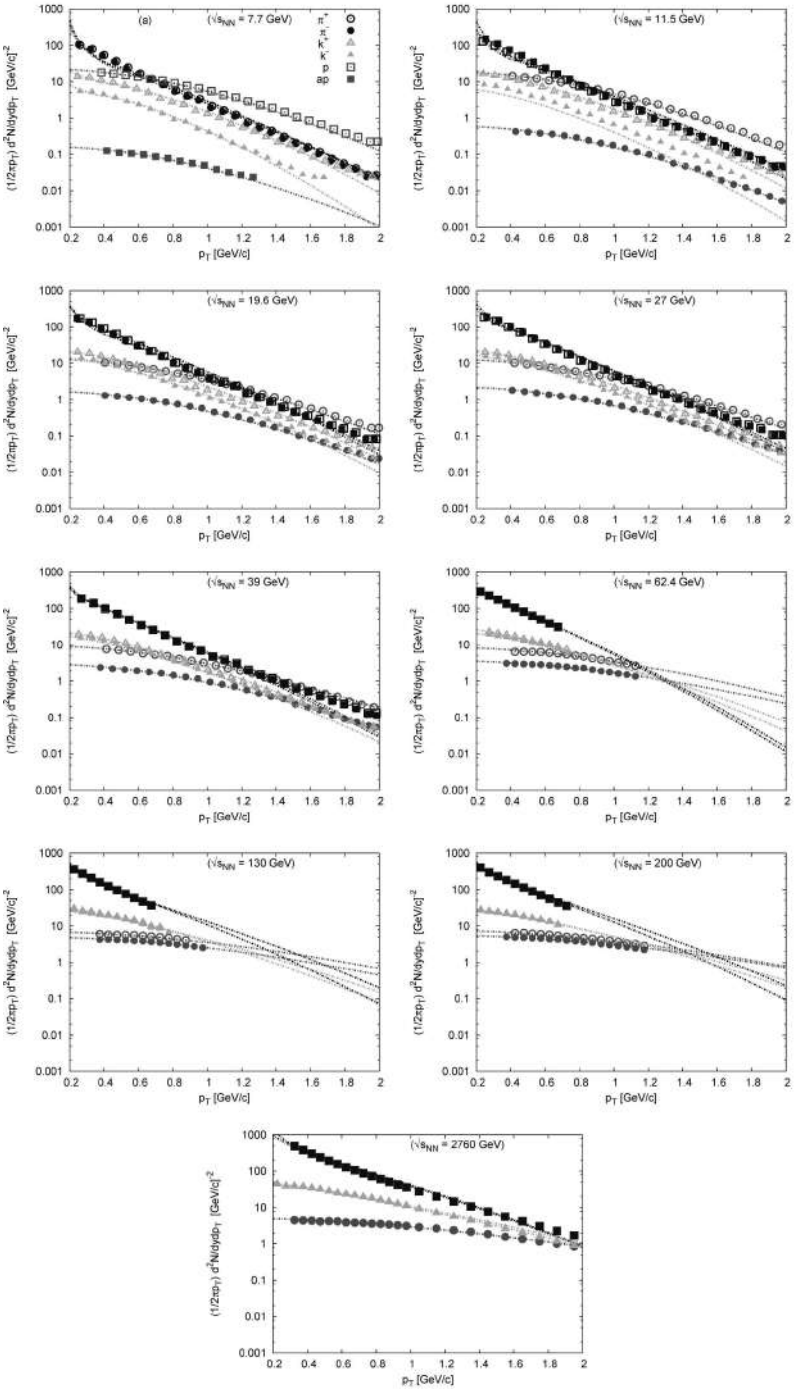

Fig. 14. Transverse momentum spectra p_{T} for charged particles measured from A + A collisions at a wide range of energies (symbols) are fitted by using the generic axiomatic statistics. Panels (a)–(i) refer to the influence of changing energies from 7.7 to 11.5 to 19.6 to 27 to 39 to 62.4 to 130 to 200 GeV and to 2.76 TeV, respectively. The corresponding fit parameters are illustrated in Figs. 2 and 3

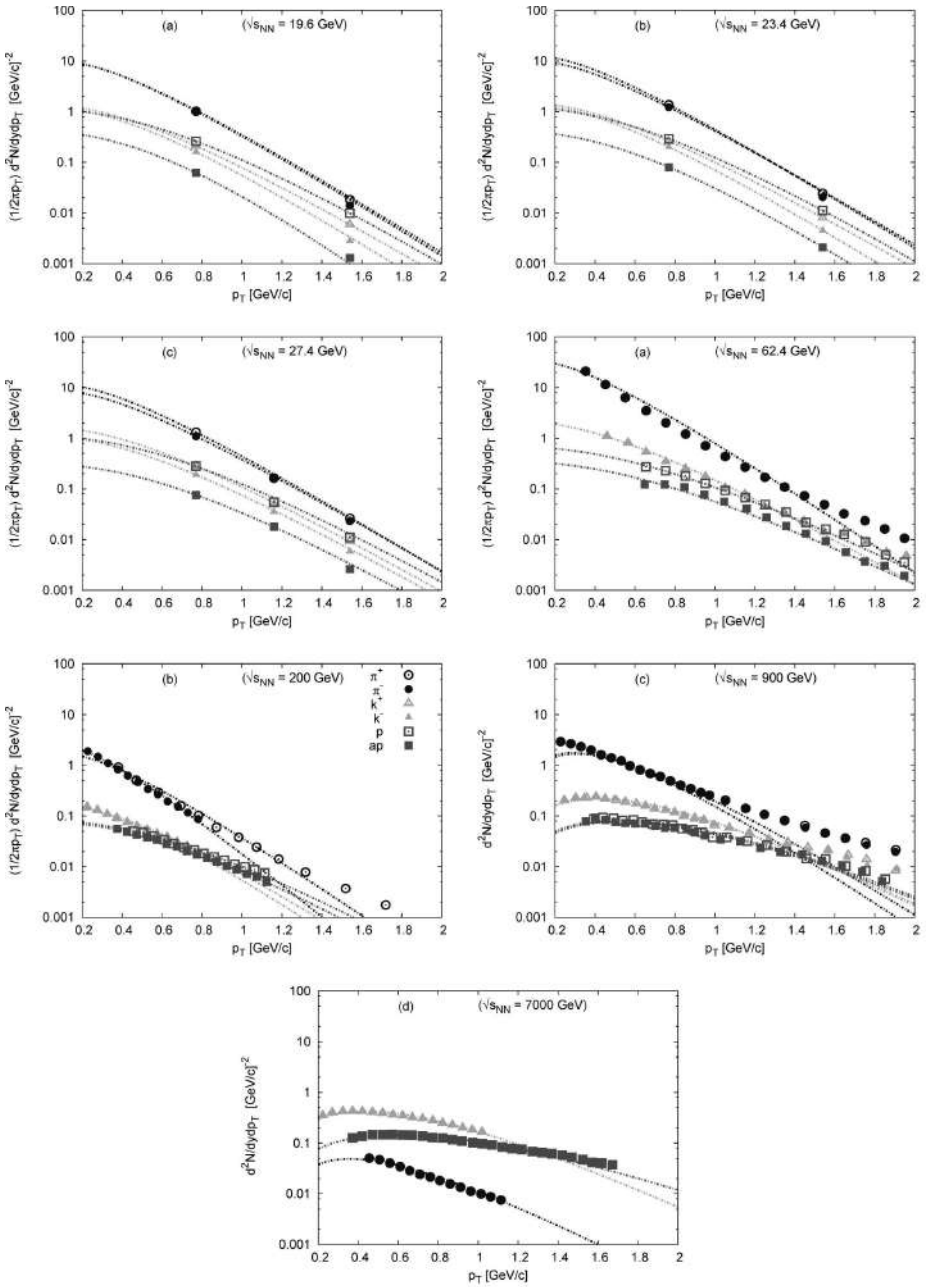

Fig. 15. The transverse momentum spectra p_{T} for charged particles measured from p + p collisions at various energies are fitted by using the Maxwell–Boltzmann statistics. Panels (a)–(g) refer to changes in the energies from 19.6 to 7 TeV, respectively. The fit parameters are presented in Fig. 7

for all particles at the whole range of energies. The resulting fit parameters are presented in Figs. 2 and 3.

c. Generic axiomatic statistical fits. Figure 14 depicts the transverse momentum spectra p_{T} for charged particles and their antiparticles measured from A + A collisions at energies ranging from 7.7 GeV to 2.76 TeV (symbols). The open symbols refer to the charged particles, while closed symbols to the antiparticles. The spectra fitted by using the generic statistics are

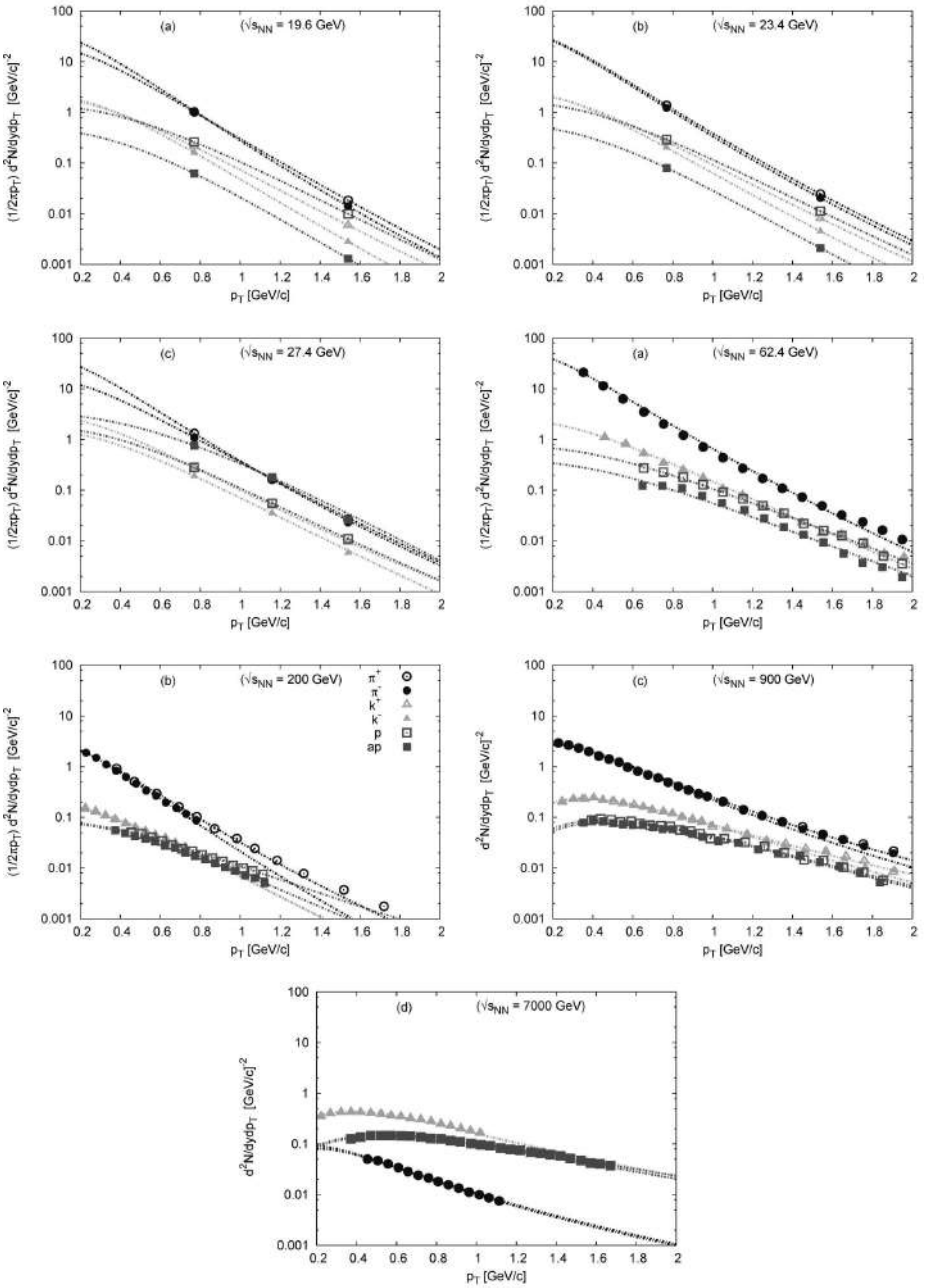

Fig. 16. The same as in Fig. 15, but by using the Tsallis statistics. The corresponding fit parameters are given in Figs. 5 and 7

given as curves. It is found that the generic axiomatic statistics reproduces well the transverse momentum distributions for all particles under study. The fit parameters are compared to the ones obtained from different types of statistics for all particles at the whole range of energies. The fit parameters are depicted in Figs. 2 and 3.

2. p + p collisions

a. Maxwell–Boltzmann statistical The transverse momentum spectra p_{T} of charged particles and their antiparticles measured in p + p collisions at energies ranging from 19.6 to 7 TeV (symbols) are fitted by the Maxwell–Boltzmann statistics (curves),

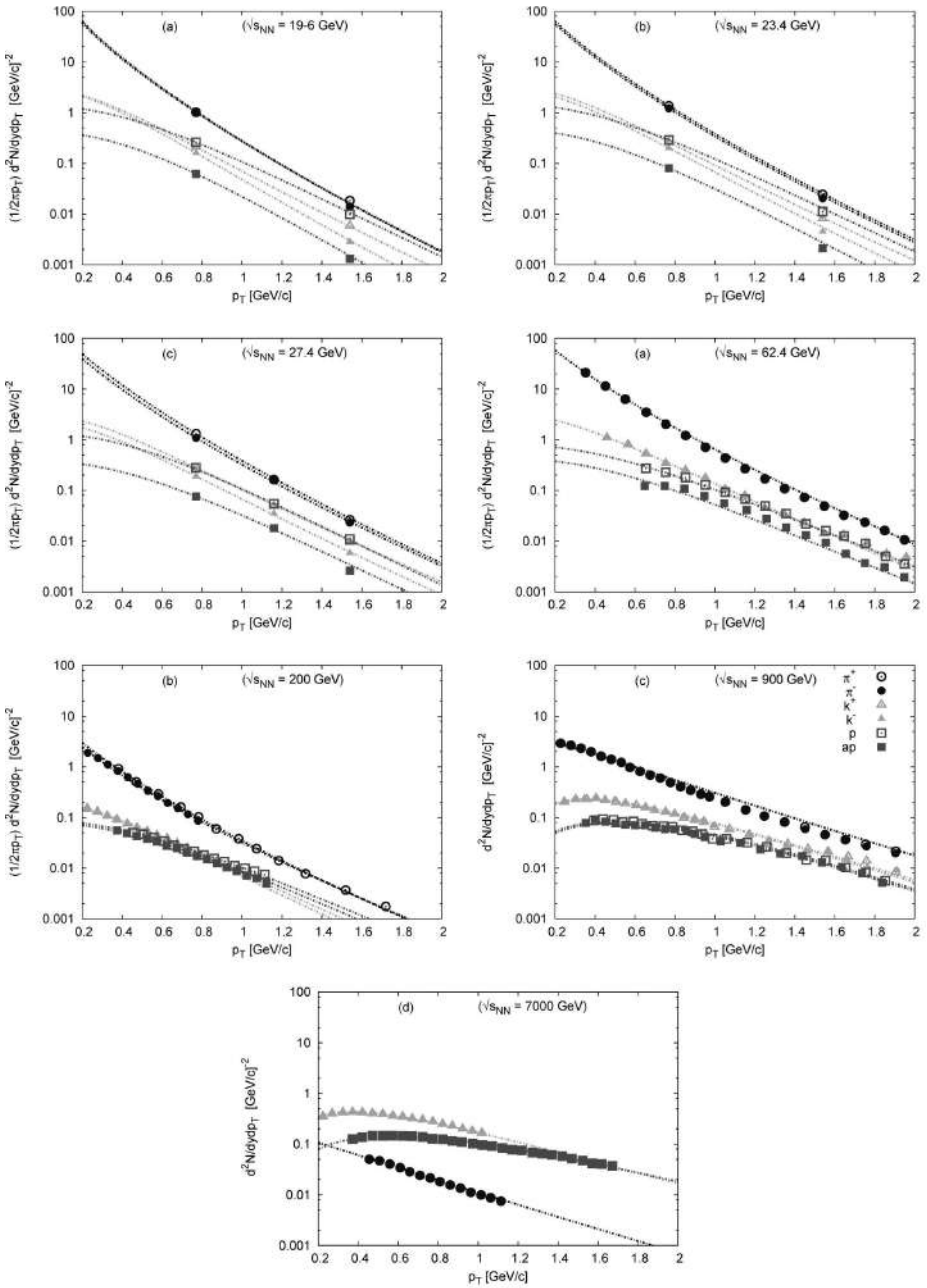

Fig. 17. The same as in Fig. 15, but by using the generic axiomatic statistics. The corresponding fit parameters are graphed in Figs. 5 and 7

Fig. 15. Symbols refer to the experimental measurements which are performed for NN collisions. It is apparent that the transverse momentum spectra p_{T} calculated within the Maxwell–Boltzmann statistics fit well the measurements for all studied particles and antiparticles. The fit parameters are depicted in Fig. 4.

b. Tsallis statistical fits. For charged particles (open symbols) and their antiparticles (open symbols) measured in p + p collisions at energies from 19.6 to 7 TeV, the transverse momentum spectra p_{T} are fitted by using the Tsallis statistics (curves) and depicted in Fig. 16. The corresponding fit parameters are depicted in Fig. 4.

c. Generic axiomatic statistical fits. At energies from 19.6 to 7 TeV, the transverse momentum spectra p_{T} calculated within the generic axiomatic statistics (curves) are fitted to measured p_{T} from p + p collisions for charged particles (open symbols) and antiparticles (solid symbols), Fig. 17. The various fit parameters are depicted in Fig. 4. With this regard, we recall that the equivalent class $c = 0.999506$ remains unchanged, in all cases.

1. A.N. Tawfik. Equilibrium statistical–thermal models in high-energy physics. *Int. J. Mod. Phys. A* **29**, 1430021 (2014).
2. A.N. Tawfik. Koppe's work of 1948: A fundamental for non-equilibrium rate of particle production. *Z. Naturforsch. A* **69**, 106 (2014).
3. E. Fermi. High energy nuclear events. *Prog. Theor. Phys.* **5**, 570 (1950).
4. E. Fermi, T. Appelquist. *Elementary Particles* (Yale University Press, 1951).
5. V.B. Magalinskii, I.P. Terletskii. The application of the microcanonical distribution to the statistical theory of multiple production of particles. *J. Exp. Theor. Phys.* **5**, 483 (1957).
6. G. Fast, R. Hagedorn. Large-angle elastic scattering at high energies treated by a statistical model. *Nuono Cimento* **27**, 208 (1963).
7. G. Fast, R. Hagedorn, L.W. Jones. A statistical interpretation of large-angle elastic scattering. *Nuovo Cimento* **27**, 856.
8. C. Tsallis. Possible generalization of Boltzmann–Gibbs statistics. *J. Statist. Phys.* **52**, 479 (1988).
9. I. Bediaga, E.M.F. Curado, J.M. de Miranda. A nonextensive thermodynamical equilibrium approach in $e^+e^- \to$ $\to$ *hadrons*. *Physica A* **286**, 156 (2000).
10. A.S. Parvan, O.V. Teryaev, J. Cleymans. Systematic comparison of Tsallis statistics for charged pions produced in pp collisions. *Eur. Phys. J. A* **53**, 102 (2017).
11. C. Beck. Non-extensive statistical mechanics and particle spectra in elementary interactions. *Physica A* **286**, 164 (2000).
12. G. Wilk, Z. Wlodarczyk. Interpretation of the nonextensitivity parameter q in some applications of Tsallis statistics and Lévy distributions. *Phys. Rev. Lett.* **84**, 2770 (2000).
13. D.B. Walton, J. Rafelski. Equilibrium distribution of heavy quarks in Fokker–Planck dynamics. *Phys. Rev. Lett.* **84**, 31 (2000).
14. W.M. Alberico, A. Lavagno, P. Quarati. Non-extensive statistics effects in quark–gluon plasma and in relativistic heavy-ion collisions. *Nucl. Phys. A* **680**, 94 (2000).
15. J. Zimányi, P. Lévai, T.S. Biró. Properties of quark matter produced in heavy-ion collision. *J. Phys. G* **31**, 711 (2005).
16. T.A. Trainor. Centrality evolution of p_t and y_t spectra from Au–Au collisions at $\sqrt{S_{NN}} = 200$ GeV. *Int. J. Mod. Phys. E* **17**, 1499 (2008).
17. G. Wilk, Z. Wlodarczyk. Power laws in elementary and heavy-ion collisions. *Eur. Phys. J. A* **40**, 299 (2009).
18. T.S. Biró, K. Ürmössy. Transverse hadron spectra from a stringy quark matter. *J. Phys. G* **36**, 064044 (2009).
19. Q.A. Wong. Extensive generalization of statistical mechanics based on incomplete information theory. *Entropy* **5**, 220 (2003).
20. S. Tripathy, T. Bhattacharyya, P. Garg, P. Kumar, R. Sahoo, J. Cleymans. Nuclear modification factor using Tsallis non-extensive statistics. *Eur. Phys. J. A* **52**, 289 (2016).
21. A. Khuntia, P. Sahoo, P. Garg, R. Sahoo, J. Cleymans. Speed of sound in hadronic matter using non-extensive Tsallis statistics. *Eur. Phys. J. A* **52**, 292 (2016).
22. T. Bhattacharyya, J. Cleymans, A. Khuntia, P. Pareek, R. Sahoo. Radial flow in non-extensive thermodynamics and study of particle spectra at LHC in the limit of small $(q-1)$. Eur. Phys. J. A **52**, 30 (2016).
23. A. Deppman. Properties of hadronic systems according to the nonextensive self-consistent thermodynamics. *J. Phys. G* **41**, 055108 (2014).
24. W.M. Alberico, P. Czerski, A. Lavagno, M. Nardi, V. Somá. Signals of non-extensive statistical mechanics in high energy nuclear collisions. *Physica A* **387**, 467 (2008).
25. A.N. Tawfik. Axiomatic nonextensive statistics at NICA energies. *Eur. Phys. J. A* **52**, 253 (2016).
26. S. Thurner, R. Hanel. Peer-review in a world with rational scientists: Toward selection of the average. *Eur. Phys. J. B* **84**, 707 (2011).
27. A.N. Tawfik, H. Yassin, E.R. Abo Elyazeed. On thermodynamic self-consistency of generic axiomatic-nonextensive statistics. *Chin. Phys. C* **41**, 053107 (2017).
28. V.F. Weisskopf. Statistics and nuclear reactions. *Phys. Rev.* **52**, 295 (1937).
29. S. Cheng, S. Pratt, P. Csizmadia, Y. Nara, D. Molnár, M. Gyulassy, S.E. Vance, B. Zhang. Effect of finite-range interactions in classical transport theory. *Phys. Rev. C* **65**, 024901 (2002).
30. A. Tounsi, K. Redlich. Canonical constraints on particle production. *J. Phys. G* **28**, 2095 (2002).
31. K. Kassner. Why ghosts don't touch: a tale of two adventurers falling one after another into a black hole. *Eur. J. Phys.* **38**, 015605 (2017).
32. H. Zheng, L. Zhu. Comparing the Tsallis distribution with and without thermodynamical description in $p+p$ collisions. *Adv. High Energy Phys.* **2016**, 9632126 (2016).
33. Y.-Q. Gao, F.-H. Liu. Comparing Tsallis and Boltzmann temperatures from relativistic heavy ion collider and large hadron collider heavy-ion data. *Indian J. Phys.* **90**, 319 (2016).
34. H. Zheng, L. Zhu. Can Tsallis distribution fit all the particle spectra produced at RHIC and LHC? *Adv. High Energy Phys.* **2015**, 180491 (2015).
35. H. Zheng, L. Zhu, A. Bonasera. Systematic analysis of hadron spectra in $p+p$ collisions using Tsallis distributions. *Phys. Rev. D* **92**, 074009 (2015).
36. G. Wilk, Z. Wlodarczyk. Tsallis distribution decorated with log-periodic oscillation. *Entropy* **17**, 384 (2015).

37. L. Marques, J. Cleymans, A. Deppman. Description of high-energy *pp* collisions using Tsallis thermodynamics: Transverse momentum and rapidity distributions. *Phys. Rev. D* **91**, 054025 (2015).
38. K. Urmossy, G.G. Barnaföldi, S. Harangozó, T.S. Biró, Z. Xu. A 'soft + hard' model for heavy-ion collisions. *J. Phys. Conf. Ser.* **805**, 012010 (2017).
39. J. Cleymans, G.I. Lykasov, A.S. Parvan, A.S. Sorin, O.V. Teryaev, D. Worku. Systematic properties of the Tsallis distribution: Energy dependence of parameters in high energy collisions. *Phys. Lett. B* **723**, 351 (2013).
40. M. Rybczyński, Z. Wlodarczyk. Tsallis statistics approach to the transverse momentum distributions in p–p collisions. *Eur. Phys. J. C* **74**, 2785 (2014).
41. A. Deppman. Self-consistency in non-extensive thermodynamics of highly excited hadronic states. *Physica A* **391**, 6380 (2012).
42. M. Kataja, P.V. Ruuskanen. Non-zero chemical potential and the shape of the p_T-distribution of hadrons in heavy-ion collisions. *Phys. Lett. B* **243**, 181 (1990).
43. S. Turbide, R. Rapp, C. Gale. Hadronic production of thermal photons. *Phys. Rev. C* **69**, 014903 (2004).
44. A. Banerjee, V.M. Yakovenko. Universal patterns of inequality. *New J. Phys.* **12**, 075032 (2010).
45. P.K. Khandai, P. Sett, P. Shukla, V. Singh. Hadron spectra in $p + p$ collisions at RHIC and LHC energies. *Int. J. Mod. Phys. A* **28**, 1350066 (2013).
46. K. Saraswat, P. Shukla, V. Singh. Strange hadron production in pp, pPb and PbPb collisions at LHC energies. *European Phys. J. A*, **53** (2017).
47. A.S. Parvan. Comparison of Tsallis statistics with the Tsallis-factorized statistics in the ultrarelativistic pp collisions. *Eur. Phys. J. A* **52**, 355 (2016).
48. F. Büyükiliç, D. Demirhan, A. Güleç. A statistical mechanical approach to generalized statistics of quantum and classical gases. *Phys. Lett. A* **197**, 209 (1995).
49. J. Stachel, A. Andronic, P. Braun-Munzinger, K. Redlich. Confronting LHC data with the statistical hadronization model. *J. Phys. Conf. Ser.* **509**, 012019 (2014).
50. S. Ban-Hao, C.-Y. Wong. Transverse-momentum distribution of produced particles in ultrarelativistic nucleus-nucleus collisions. *Phys. Rev. D* **32**, 1706 (1985).
51. P. Danielewicz, M. Gyulassy. Dissipative phenomena in quark-gluon plasmas. *Phys. Rev. D* **31**, 53 (1985).
52. P.J. Siemens, J.O. Rasmussen. Evidence for a blast wave from compressed nuclear matter. *Phys. Rev. Lett.* **42**, 880 (1979).
53. G.D. Westfall, J. Gosset, P.J. Johansen, A.M. Poskanzer, W.G. Meyer, H.H. Gutbrod, A. Sandoval, R. Stock. Nuclear fireball model for proton inclusive spectra from relativistic heavy-ion collisions. *Phys. Rev. Lett.* **37**, 1202 (1976).
54. E. Schnedermann, J. Sollfrank, U.W. Heinz. Thermal phenomenology of hadrons from 200A GeV S + S collisions. *Phys. Rev. C* **48**, 2462 (1993).
55. C. Anderlik, Zs.I. Lázár, V.K. Magas, L.P. Csernai, H. Stöcker, W. Greiner. Nonideal particle distributions from kinetic freeze-out models. *Phys. Rev. C* **59**, 388 (1999).
56. I.P. Lokhtin, A.M. Snigirev. A model of transverse expansion of the quark-gluon fluid with phase transition and hadron spectra in heavy ion collisions. *Phys. Lett. B* **378**, 247 (1996).
57. T.D. Biro. *Is there a temperature: Conceptual Challenges at High Energy, Acceleration and Complexity* (Springer-Verlag, 2011).
58. H.-R. Wei, F.-H. Liu, R.A. Lacey. Kinetic freeze-out temperature and flow velocity extracted from transverse momentum spectra of final-state light flavor particles produced in collisions at RHIC and LHC. *Eur. Phys. J. A* **52**, 102 (2016).
59. H.-L. Lao, H.-R. Wei, F.-H. Liu, R.A. Lacey. An evidence of mass-dependent differential kinetic freeze-out scenario observed in Pb–Pb collisions at 2.76 TeV. *Eur. Phys. J. A* **52**, 203 (2016).
60. P. Huovinen, P.V. Ruuskanen. Hydrodynamic models for heavy ion collisions. *Ann. Rev. Nucl. Part. Sci.* **56**, 163 (2006).
61. L. Adamczyk *et al.* (STAR Collaboration). Bulk properties of the medium produced in relativistic heavy-ion collisions from the beam energy scan program. *Phys. Rev. C* **96**, 044904 (2017).
62. B.I. Abelev *et al.* (STAR Collaboration). Systematic measurements of identified particle spectra in *pp*, $d+$Au, and Au + Au collisions at the STAR detector. *Phys. Rev. C* **79**, 034909 (2009).
63. A. Bialas. Tsallis $p_\perp$ distribution from statistical clusters. *Phys. Lett. B* **747**, 190 (2015).
64. M. Gyulassy, I. Vitev, X.-N. Wang, B.-W. Zhang. Jet quenching and radiative energy loss in dense nuclear matter. In: *Quark Gluon Plasma*. Edited by R.C. Hwa, X.-N. Wang (World Scientific, 2003), pp. 123–191.
65. D. d'Enterria. Relevance of baseline hard proton–proton spectra for high-energy nucleus–nucleus physics. *J. Phys. G* **31**, S491 (2005).
66. K. Adcox *et al.* (PHENIX Collaboration). Suppression of hadrons with large transverse momentum in central Au + Au collisions at $\sqrt{s_{NN}} = 130$ GeV. *Phys. Rev. Lett.* **88**, 022301 (2002).
67. C. Adler *et al.* (STAR Collaboration). Centrality dependence of high-p_T hadron suppression in Au + Au collisions at $\sqrt{s_{NN}} = 130$ GeV. *Phys. Rev. Lett.* **89**, 202301 (2002).
68. S.S. Adler *et al.* (PHENIX Collaboration). Suppressed π^0 production at large transverse momentum in central Au + Au collisions at $\sqrt{s_{NN}} = 200$ GeV. *Phys. Rev. Lett.* **91**, 072301 (2003).
69. J. Adams *et al.* (STAR Collaboration). Transverse-momentum and collision-energy dependence of high-p_T hadron suppression in Au + Au collisions at ultrarelativistic energies. *Phys. Rev. Lett.* **91**, 172302 (2003).
70. B.B. Back, M.D. Baker, D.S. Barton, R.R. Betts, M. Ballintijn, A.A. Bickley, R. Bindel, A. Budzanowski, W. Busza, A. Carroll, M.P. Decowski, N. George, K. Gulbrandsen, S. Gushue, C. Halliwell *et al.* Charged hadron

transverse momentum distributions in Au + Au collisions at $\sqrt{s_{NN}} = 200$ GeV. *Phys. Lett. B* **578**, 297 (2004).
71. I. Arsene *et al.* (BRAHMS Collaboration). Transverse-momentum spectra in Au + Au and d + Au collisions at $\sqrt{s_{NN}} = 200$ GeV and the pseudorapidity dependence of high-p_T suppression. *Phys. Rev. Lett.* **91**, 072305 (2003).
72. S.S. Adler *et al.* (PHENIX Collaboration). Midrapidity neutral-pion production in proton-proton collisions at $\sqrt{s_{NN}} = 200$ GeV. *Phys. Rev. Lett.* **91**, 241803 (2003).
73. M.M. Aggarwal *et al.* (WA98 Collaboration). Transverse mass distributions of neutral pions from ^{208}Pb-induced reactions at 158A GeV. *Eur. Phys. J. C* **23**, 225 (2002).
74. M.M. Aggarwal *et al.* (WA98 Collaboration). Three-pion interferometry results from central Pb + Pb collisions at 158A GeV/c. *Phys. Rev. Lett.* **85**, 2985 (2000).
75. M.M. Aggarwal *et al.* (WA98 Collaboration). Centrality dependence of neutral pion production in 158A GeV ^{208}Pb + ^{208}Pb collisions. *Phys. Rev. Lett.* **81**, 4087 (1998) [Erratum: *Phys. Rev. Lett.* **84**, 578 (2000)].
76. X.-N. Wang. Where is the jet quenching in Pb + Pb collisions at 158A GeV? *Phys. Rev. Lett.* **81**, 2655 (1998).
77. X.-N. Wang. Systematic study of high p_T hadron spectra in pp, pA, and AA collisions at ultrarelativistic energies. *Phys. Rev. C* **61**, 064910 (2000).
78. E. Wang, X.-N. Wang. Interplay of soft and hard processes and hadron p_T spectra in pA and AA collisions. *Phys. Rev. C* **64**, 034901 (2001).
79. J.W. Cronin, H.J. Frisch, M.J. Shochet, J.P. Boymond, P.A. Piroué, R.L. Sumner. Production of hadrons at large transverse momentum at 200, 300, and 400 GeV. *Phys. Rev. D* **11**, 3105 (1975).
80. B.Z. Kopeliovich, J. Nemchik, A. Schäfer, A.V. Tarasov. Cronin effect in hadron production off nuclei. *Phys. Rev. Lett.* **88**, 232303 (2002).
81. V.N. Gribov, B.L. Ioffe, I.Ya. Pomeranchuk. On the total annihilation cross-section of electron–positron pairs into hadrons at high-energies. *Sov. J. Nucl. Phys.* **6**, 427 (1968) [*Phys. Lett.* **24B**, 554 (1967)].
82. K. Geiger. Quantum field kinetics of QCD: Quark-gluon transport theory for light-cone-dominated processes. *Phys. Rev. D* **54**, 949 (1996).
83. A. Ayala, J. Jalilian-Marian, L.D. McLerran, R. Venugopalan. Gluon propagator in non-Abelian Weizsäcker–Williams fields. *Phys. Rev. D* **52**, 2935 (1995).
84. Z.-T. Liang, X.-N. Wang. Globally polarized quark-gluon plasma in noncentral A + A collisions. *Phys. Rev. Lett.* **94**, 102301 (2005) [Erratum: *Phys. Rev. Lett.* **96**, 039901 (2006)].
85. M. Diehl, J.R. Gaunt. Chapter 2: Double parton scattering theory overview. *Adv. Ser. Direct. High Energy Phys.* **29**, 7 (2018).
86. T. Kasemets, S. Scopetta. Chapter 4: Parton correlations in double parton scattering. *Adv. Ser. Direct. High Energy Phys.* **29**, 49 (2018).
87. D. Antreasyan, J.W. Cronin, H.J. Frisch, M.J. Shochet, L. Kluberg, P.A. Piroué, R.L. Sumner. Production of hadrons at large transverse momentum in 200-, 300-, and 400-GeV p–p and p-nucleus collisions. *Phys. Rev. D* **19**, 764 (1979).
88. P.B. Straub, D.E. Jaffe, H.D. Glass, M.R. Adams, C.N. Brown, G. Charpak, W.E. Cooper, J.A. Crittenden, D.A. Finley, R. Gray, Y. Hemmi, Y.B. Hsiung, J.R. Hubbard, A.M. Jonckheere, H. Jöstlein *et al.* Nuclear dependence of high-x_t hadron and high-T hadron-pair production in p-A interactions at $\sqrt{s} = 38.8$ GeV. *Phys. Rev. Lett.* **68**, 452 (1992).
89. A.L.S. Angelis *et al.* (BCMOR Collaboration). Large transverse momentum π^0 production in $\alpha\alpha$, dd and pp collisions at the CERN ISR. *Phys. Lett. B* **185**, 213 (1987).
90. B.B. Abelev *et al.* (ALICE Collaboration). Energy dependence of the transverse momentum distributions of charged particles in pp collisions measured by ALICE. *Eur. Phys. J. C* **73**, 2662 (2013).
91. R. Sassot, P. Zurita, M. Stratmann. Inclusive hadron production in the CERN-LHC era. *Phys. Rev. D* **82**, 074011 (2010).
92. S. Chatrchyan *et al.* (CMS Collaboration). Study of the inclusive production of charged pions, kaons, and protons in pp collisions at $\sqrt{s} = 0.9$, 2.76, and 7 TeV. *Eur. Phys. J. C* **72**, 2164 (2012).
93. K. Aamodt *et al.* (ALICE Collaboration). Production of pions, kaons and protons in pp collisions at $\sqrt{s} = 900$ GeV with ALICE at the LHC. *Eur. Phys. J. C* **71**, 1655 (2011).
94. V. Khachatryan *et al.* (CMS Collaboration). Transverse-momentum and pseudorapidity distributions of charged hadrons in pp collisions at $\sqrt{s} = 0.9$ and 2.36 TeV. *JHEP* **02**, 041 (2010).
95. V. Khachatryan *et al.* (CMS Collaboration). Transverse-momentum and pseudorapidity distributions of charged hadrons in pp collisions at $\sqrt{s} = 7$ TeV. *Phys. Rev. Lett.* **105**, 022002 (2010).
96. J. Adams *et al.* (STAR Collaboration). $K(892)^*$ resonance production in Au + Au and $p + p$ collisions at $\sqrt{s_{NN}} = 200$ GeV. *Phys. Rev. C* **71**, 064902 (2005).
97. T.S. Biró, G. Purcsel, K. Ürmössy. Non-extensive approach to quark matter. *Eur. Phys. J. A* **40**, 325 (2009).
98. F.-H. Liu. Unified description of multiplicity distributions of final-state particles produced in collisions at high energies. *Nucl. Phys. A* **810**, 159 (2008).
99. F.-H. Liu, J.-S. Li. Isotopic production cross section of fragments in ^{56}Fe + p and ^{136}Xe(^{124}Xe) + Pb reactions over an energy range from 300A to 1500A MeV. *Phys. Rev. C* **78**, 044602 (2008).
100. F.-H. Liu, Y.-Q. Gao, T. Tian, B.-C. Li. Unified description of transverse momentum spectrums contributed by soft and hard processes in high-energy nuclear collisions. *Eur. Phys. J. A* **50**, 94 (2014).
101. Y.-Q. Gaoa, C.-X. Tiana, F.-H. Liua, M.A. Rahimb, S. Fakhraddin. Transverse momentum distributions of identified particles produced in pp, $p(d)A$, and AA collisions at high energies. *PRAMANA J. phys.* **79**, 1407 (2012).
102. H.-R. Wei, F.-H. Liu. A study of transverse momentum distributions of jets produced in p-p, p-$\bar{p}$, d-Au, Au-Au,

and Pb-Pb collisions at high energies. *Adv. High Energy Phys.* **2015**, 263135 (2015).
103. H.-R. Wei, F.-H. Liu, R.A. Lacey. Disentangling random thermal motion of particles and collective expansion of source from transverse momentum spectra in high energy collisions. *J. Phys. G* **43**, 125102 (2016).
104. S.S. Adler *et al.* (PHENIX Collaboration). Identified charged particle spectra and yields in Au + Au collisions at $\sqrt{s_{NN}} = 200$ GeV. *Phys. Rev. C* **69**, 034909 (2004).
105. S. Takeuchi, K. Murase, T. Hirano, P. Huovinen, Y. Nara. Effects of hadronic rescattering on multistrange hadrons in high-energy nuclear collisions. *Phys. Rev. C* **92**, 044907 (2015).
106. H. Heiselberg, A.-M. Levy. Elliptic flow and Hanbury-Brown–Twiss correlations in noncentral nuclear collisions. *Phys. Rev. C* **59**, 2716 (1999).
107. U.W. Heinz. Concepts of heavy ion physics. In: *Proceedings of 2002 European School of high-energy physics, Pylos, Greece, 25 Aug–7 Sep 2002* (2004), pp. 165–238.
108. R. Russo. *Measurement of D^+ meson production in p-Pb collisions with the ALICE detector*. PhD thesis (Turin Univer., 2015).
109. J. Adam *et al.* (ALICE Collaboration). Measurement of pion, kaon and proton production in proton–proton collisions at $\sqrt{s} = 7$ TeV. *Eur. Phys. J. C* **75**, 226 (2015).
110. C. Andrei. Light flavor hadron spectra at low p_T and search for collective phenomena in high multiplicity pp, p–Pb and Pb–Pb collisions measured with the ALICE experiment *Nucl. Phys. A* **931**, 888 (2014).
111. N. Suzuki, M. Biyajima. Transverse momentum distribution with radial flow in relativistic diffusion model. *Int. J. Mod. Phys. E* **E16**, 133 (2007).
112. F.-H. Liu, Y.-Q. Gao, B.C. Li. Comparing two-Boltzmann distribution and Tsallis statistics of particle transverse momentums in collisions at LHC energies. *Eur. Phys. J. A* **50**, 123 (2014).
113. H. Yassin, E.R. Abo Elyazeed. Transverse momentum p_T spectra of strange particles production in different collisions at $\sqrt{s_{NN}} = 2.76$,5.02, and 7 TeV. *Acta Phys. Pol. B* **50**, 37 (2018).
114. C. Anteneodo, A.R. Plastino. Maximum entropy approach to stretched exponential probability distributions. *J. Phys. A: Math. Gen.* **32**, 1089 (1999).
115. A.N. Tawfik, H. Yassin, E.R. Abo Elyazeed. Chemical freezeout parameters within generic nonextensive statistics. *Indian J. Phys.* **92**, 1325 (2018).
116. M. Banner *et al.* (UA2 Collaboration). Inclusive charged particle production at the CERN $\bar{p}p$ collider. *Phys. Lett.* **122B**, 322 (1983).
117. T. Alexopoulos *et al.* (E735 Collaboration). Mass-identified particle production in proton-antiproton collisions at $\sqrt{s_{NN}} = 300$, 540, 1000, and 1800 GeV. *Phys. Rev. D* **48**, 984 (1993).
118. A. Adare *et al.* (PHENIX Collaboration). Identified charged hadron production in $p+p$ collisions at $\sqrt{s_{NN}} =$ $= 200$ and 62.4 GeV. *Phys. Rev. C* **83**, 064903 (2011).
119. B.I. Abelev *et al.* (STAR Collaboration). Strange particle production in $p+p$ collisions at $\sqrt{s_{NN}} = 200$ GeV. *Phys. Rev. C* **75**, 064901 (2007).
120. B.I. Abelev *et al.* (STAR Collaboration). Energy dependence of $\pi^{\pm}$, p and $\bar{p}$ transverse momentum spectra for Au + Au collisions at $\sqrt{s_{NN}} = 62.4$ and 200 GeV. *Phys. Lett. B* **655**, 104 (2007).
121. A. Adare *et al.* (PHENIX Collaboration). Spectra and ratios of identified particles in Au + Au and d+Au collisions at $\sqrt{s_{NN}} = 200$ GeV. *Phys. Rev. C* **88**, 024906 (2013).
122. B. Abelev *et al.* (ALICE Collaboration). Pion, kaon, and proton production in central Pb–Pb collisions at $\sqrt{s_{NN}} =$ $= 2.76$ TeV. *Phys. Rev. Lett.* **109**, 252301 (2012).
123. P. Sett, P. Shukla. Pion p_T spectra in $p+p$ collisions as a function of $\sqrt{s}$ and event multiplicity. *Adv. High Energy Phys.* **2014**, 896037 (2014).
124. W.M. Alberico, A. Lavagno. Non-extensive statistical effects in high-energy collisions. *Eur. Phys. J. A* **40**, 313 (2009).
125. J. Adams *et al.* (STAR Collaboration.) Identified hadron spectra at large transverse momentum in $p+p$ and $d+$Au collisions at $\sqrt{s_{NN}} = 200$ GeV. *Phys. Lett. B* **637**, 161 (2006.)

Received 05.01.21

Х. Яссін, А.Н. Тавфік, Е.Р. Або Елязід

ЕКСТЕНСИВНІ/НЕЕКСТЕНСИВНІ СТАТИСТИКИ ДЛЯ p_{T} РОЗПОДІЛІВ РІЗНИХ ЗАРЯДЖЕНИХ ЧАСТИНОК, НАРОДЖЕНИХ У p + p ТА A + A ЗІТКНЕННЯХ У ШИРОКОМУ ДІАПАЗОНІ ЕНЕРГІЙ

Представлено вичерпний огляд експериментальних параметризацій, запропонованих для опису розподілів поперечного імпульсу заряджених піонів, каонів та протонів, що народжуються в діапазоні енергії від 7,7 ГеВ до 2,76 ТеВ. Досліджено статистичні підгонки з екстенсивною статистикою Максвела–Больцмана (МБ) або неекстенсивною (загальною аксіоматичною статистикою і окремо статистикою Цалліса). Обговорюється питання невідповідності між тим, що розподіл МБ описує хімічний фрізаут, тоді як статистика Цалліса – кінетичний фрізаут. Залежності параметрів підгонки від енергії суттєво різні для різних типів частинок і різного ступеня (не)екстенсивності. Це проявляється в тому, що неекстенсивний підхід Цалліса є більш придатним для p + p, ніж для A + A зіткнень. Хоча обговорення більш глибокого фізичного змісту неекстенсивних статистичних підходів не є нашою метою, ми надаємо повну картину використання статистики Цалліса в моделюванні розподілів поперечних імпульсів кількох заряджених частинок, що утворюються в широкому діапазоні енергій, і висловлюємо критику чи підтримку відповідних робіт.

Ключові слова: неекстенсивна термодинамічна узгодженість, загальна (не)екстенсивна статистика, статистики Больцмана і Фермі–Дірака.